

# UNCLASSIFIED

AD NUMBER
AD275107
NEW LIMITATION CHANGE
TO Approved for public release, distribution unlimited
FROM Distribution authorized to U.S. Gov't. agencies and their contractors; Administrative/Operational Use; FEB 1962. Other requests shall be referred to Aeronautical Systems Division, Wright-Patterson AFB, OH 45433.
AUTHORITY
ASD ltr dtd 26 Jul 1966

THIS PAGE IS UNCLASSIFIED

**UNCLASSIFIED**

---

**AD 275 107**

*Reproduced  
by the*

**ARMED SERVICES TECHNICAL INFORMATION AGENCY  
ARLINGTON HALL STATION  
ARLINGTON 12, VIRGINIA**



---

**UNCLASSIFIED**

NOTICE: When government or other drawings, specifications or other data are used for any purpose other than in connection with a definitely related government procurement operation, the U. S. Government thereby incurs no responsibility, nor any obligation whatsoever; and the fact that the Government may have formulated, furnished, or in any way supplied the said drawings, specifications, or other data is not to be regarded by implication or otherwise as in any manner licensing the holder or any other person or corporation, or conveying any rights or permission to manufacture, use or sell any patented invention that may in any way be related thereto.

275107

275 107

ASD TECHNICAL REPORT 61-712

CATALOGED BY ASTIA  
AS AD NO. \_\_\_\_\_

EXPERIMENTAL AND THEORETICAL INVESTIGATION OF THE FLUTTER  
CHARACTERISTICS OF A MODEL HELICOPTER ROTOR BLADE IN FORWARD FLIGHT

Charles A. Gates

Frank A. DuWaldt

CORNELL AERONAUTICAL LABORATORY, INC.

Buffalo 21, New York

February 1962

AERONAUTICAL SYSTEMS DIVISION

NO OTS

**Best  
Available  
Copy**

## NOTICES

When Government drawings, specifications, or other data are used for any purpose other than in connection with a definitely related Government procurement operation, the United States Government thereby incurs no responsibility nor any obligation whatsoever; and the fact that the Government may have formulated, furnished, or in any way supplied the said drawings, specifications, or other data, is not to be regarded by implication or otherwise as in any manner licensing the holder or any other person or corporation, or conveying any rights or permission to manufacture, use, or sell any patented invention that may in any way be related thereto.

ASTIA release to OTS not authorized.

Qualified requesters may obtain copies of this report from the Armed Services Technical Information Agency, (ASTIA), Arlington Hall Station, Arlington 12, Virginia.

Copies of ASD Technical Reports and Technical Notes should not be returned to the Aeronautical Systems Division unless return is required by security considerations, contractual obligations, or notice on a specific document.

ASD TECHNICAL REPORT 61-712

EXPERIMENTAL AND THEORETICAL INVESTIGATION OF THE FLUTTER  
CHARACTERISTICS OF A MODEL HELICOPTER ROTOR BLADE IN FORWARD FLIGHT

Charles A. Gates  
Frank A. DuWaldt

CORNELL AERONAUTICAL LABORATORY, INC.  
Buffalo 21, New York

February 1962

Contract No. AF 33(616)-7669  
Project No. 3137  
Task No. 313704

AERONAUTICAL SYSTEMS DIVISION  
AIR FORCE SYSTEMS COMMAND  
UNITED STATES AIR FORCE  
WRIGHT-PATTERSON AIR FORCE BASE, OHIO

## FOREWORD

The work reported herein was accomplished at the Cornell Aeronautical Laboratory, Inc., in Buffalo, New York, under U. S. Air Force Contract No. AF 33(616)-7669, Project No. 3137, Task No. 313704, "Study of the Problems Associated with Flutter of Rotor Blades in Forward Flight". Mr. H. Cochran, Branch Chief V/STOL Propulsion Branch, ASD, was the project monitor. The Transportation Research Command (TRECOM) of the Army Transportation Corp supported the effort.

## ABSTRACT

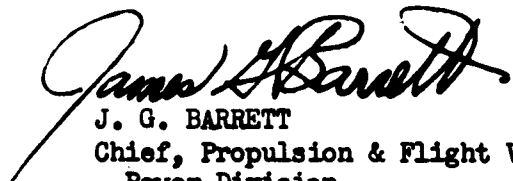
An experimental and analytical investigation was made of the effects of advance ratio on the flutter characteristics of a model helicopter rotor blade. Analyses were based on linearized equations of motion for the flapping, pitching, bending and twisting degrees of freedom although twisting was neglected in the subsequent calculations. Reversed flow effects were included in the evaluation of the aerodynamic forces.

Experimental flutter data were obtained by testing a model helicopter rotor blade mounted on the CAL/TRECOM Small Rotorcraft Test Apparatus. These data were compared with the results of calculations based on the linearized equations of motion for pitching, flapping and bending. The trends of the theoretical and experimental results were in fair agreement. Lack of good quantitative agreement is believed to be caused by the absence of an adequate unsteady aerodynamic theory.

## PUBLICATION REVIEW

This report has been reviewed and is approved.

FOR THE COMMANDER:



J. G. BARRETT  
Chief, Propulsion & Flight Vehicle  
Power Division  
Directorate of Defense & Transport  
Systems Engineering

## SUMMARY

An experimental and analytical investigation was made of the effects of advance ratio on the flutter characteristics of a model helicopter rotor blade.

Flutter tests were made with the model mounted on the CAL/TRECOM Small Rotorcraft Test Apparatus at advance ratios from 0 to 0.7. Rotor shaft angle, collective pitch angle, blade c. g. location, and pitch restraint were varied.

Linearized equations of motion were used to represent the dynamics of the rotor blade. Reversed-flow effects were included in the quasi-steady theory used in the development of the aerodynamic coefficients.

To determine the theoretical stability boundaries, an analog computer was used to solve the coupled pitching, flapping and bending equations of motion. Increased advance ratio generally decreased the rotor rotational speed at which the instability occurred. The magnitude of the effect of advance ratio depended on the blade unbalance (i. e., chordwise c. g. position) and the ratio of bending frequency to pitching frequency.

Agreement between theoretical and experimental data was only qualitative.

## TABLE OF CONTENTS

	<u>Page No.</u>
I. INTRODUCTION	1
II. TEST APPARATUS	4-
III. FLUTTER EXPERIMENTS	6
A. Technique	6
B. Range of Experiments	6
C. Experimental Flutter Results	7
IV. DISCUSSION OF ANALYSES	9
A. Equations of Motion	9
B. Derivation of Aerodynamic Coefficients for Reverse Flow	9
C. Flutter Calculations	11
V. COMPARISON OF EXPERIMENTAL AND CALCULATED RESULTS	14
VI. CONCLUSIONS	15
VII. RECOMMENDATIONS	16
APPENDIX I      Model Physical Characteristics	17
APPENDIX II     Equations of Motion and Generalized Coefficients	21
REFERENCES	60

# LIST OF ILLUSTRATIONS

<u>Figure No.</u>		<u>Page No.</u>
1a	Helicopter Flutter Model Installation on Small Rotorcraft Test Apparatus - Side View	35
1b	Helicopter Flutter Model Installation on Small Rotorcraft Test Trailer - View Looking Forward	36
2	Small Rotorcraft Test Trailer	37
3	Tractor for Small Rotorcraft Test Apparatus	38
4	Head - Helicopter Flutter Model	39
5	Rotor Hydraulic Pump	40
6	Instrumentation and Control Panels - Small Rotorcraft Test Trailer	41
7	Approximate Stall Regions for Retreating Blade Tip of the Model Rotor as Functions of Collective Pitch and Rotor Shaft Tilt	42
8	Experimental Flutter Data: <u>Nonrotating Pitching Frequency</u> vs. Advance Ratio	
a)	$\bar{x}_E / c = 0.0036, \bar{\omega}_\phi / \bar{\omega}_{\theta_0} = 1.03 \text{ and } 1.44; 3^\circ < \theta_0 < 4^\circ$	43
b)	$\bar{x}_E / c = 0.044, \bar{\omega}_\phi / \bar{\omega}_{\theta_0} = 1.05 \text{ and } \bar{x}_E / c = 0.039$ $\bar{\omega}_\phi / \bar{\omega}_{\theta_0} = 1.09; 3.5^\circ < \theta_0 < 5.5^\circ$	44
c)	$\bar{x}_E / c = 0.057, \bar{\omega}_\phi / \bar{\omega}_{\theta_0} = 0.71, 1.00, \text{ and } 1.20;$ $2^\circ < \theta_0 < 6^\circ$	45
d)	$\bar{x}_E / c = 0.057, \bar{\omega}_\phi / \bar{\omega}_{\theta_0} = 0.71 \text{ and } 1.00; 7^\circ < \theta_0 < 8^\circ$	46
e)	$\bar{x}_E / c = 0.139, \bar{\omega}_\phi / \bar{\omega}_{\theta_0} = 0.63 \text{ and } 1.31; \theta_0 \approx 4^\circ$	47

LIST OF ILLUSTRATIONS  
(continued)

<u>Figure No.</u>		<u>Page No.</u>
9	Calculated Flutter Boundaries: <u>Nonrotating Pitching Frequency</u> vs. Advance Ratio Shaft Rotational Speed	
	a) $\bar{\gamma}_E / C$ = 0.0036, $\bar{\omega}_\phi / \bar{\omega}_{\theta_0}$ = 1.45	48
	b) $\bar{\gamma}_E / C$ = 0.0036, $\bar{\omega}_\phi / \bar{\omega}_{\theta_0}$ = 1.04	49
	c) $\bar{\gamma}_E / C$ = 0.0036, $\bar{\omega}_\phi / \bar{\omega}_{\theta_0}$ = 0.585	50
	d) $\bar{\gamma}_E / C$ = 0.044, $\bar{\omega}_\phi / \bar{\omega}_{\theta_0}$ = 1.44	51
	e) $\bar{\gamma}_E / C$ = 0.044, $\bar{\omega}_\phi / \bar{\omega}_{\theta_0}$ = 0.95	52
	f) $\bar{\gamma}_E / C$ = 0.044, $\bar{\omega}_\phi / \bar{\omega}_{\theta_0}$ = 0.58	53
	g) $\bar{\gamma}_E / C$ = 0.139, $\bar{\omega}_\phi / \bar{\omega}_{\theta_0}$ = 1.55	54
	h) $\bar{\gamma}_E / C$ = 0.139, $\bar{\omega}_\phi / \bar{\omega}_{\theta_0}$ = 1.11	55
	i) $\bar{\gamma}_E / C$ = 0.139, $\bar{\omega}_\phi / \bar{\omega}_{\theta_0}$ = 0.63	56
10	Comparison of Experimental and Calculated Flutter Boundaries: <u>Nonrotating Pitching Frequency</u> vs. Advance Ratio Shaft Rotational Speed	
	a) $\bar{\gamma}_E / C$ = 0.0036	57
	b) $\bar{\gamma}_E / C$ = 0.044 and 0.039	58
	c) $\bar{\gamma}_E / C$ = 0.139	59

# LIST OF TABLES

<u>Table No.</u>		<u>Page No.</u>
I.1	C.A.L. Blade Model 4 - Section Mass and Stiffness Properties.....	18
I.2	Blade and Hub Properties - C.A.L. Blade Model 4 - No Pod.....	19
I.3	Hub Inertial Characteristics.....	20
II.1	Equations of Motion.....	22
II.2	Generalized Mass Coefficients.....	23
II.3	Generalized Centrifugal Force Coefficients.....	24
II.4	Generalized Gyroscopic Coupling Coefficients.....	25
II.5	Generalized Aerodynamic Coefficients.....	26

# LIST OF SYMBOLS

$\left. \begin{matrix} A_{ij} \\ C_{ij} \\ D_{ij} \\ S_{ij} \\ S'_{ij} \\ S''_{ij} \end{matrix} \right\}$	= Aerodynamic Coefficients (APPENDIX II)
$a$	= Lift curve slope, $(\text{rad})^{-1} = a_{M=0} / \sqrt{1-M_{0.8}^2}$
$a_{RF}$	= Lift curve slope in reversed flow region, $(\text{rad})^{-1}$
$a_i = \frac{-\tau_{ii}}{m_{ii}}$	= Southwell coefficient for $i^{\text{th}}$ mode, nondimensional
$B$	= Tip-loss factor (aerodynamic lift and induced drag forces neglected outboard of Sta.BR), nondimensional
$b$	= Semichord, ft.
$C_D$	= Profile drag coefficient, nondimensional
$f_{\phi_n}$	= Bending deflection shape normalized to unit tip deflection for the $n^{\text{th}}$ mode, nondimensional
$f_{\phi_n}^*$	= Bending deflection shape referred to root chord plane for the $n^{\text{th}}$ mode, nondimensional
$G_{ij}$	= Gyroscopic coupling coefficient*
$I_{x_1}$	= Total moment of inertia about elastic axis due to chordwise mass distribution, slugs $\text{ft.}^2$
$I_r$	= Total moment of inertia about flapping axis due to spanwise mass distribution, slugs $\text{ft.}^2$

---

\* Units determined by equation and term

LIST OF SYMBOLS  
(continued)

$I_{z,}$	=	Moment of inertia of blade and blade retention due to mass distribution normal to chord plane (does not include effect of initial bending deflection), slugs ft. <sup>2</sup>
$I_{z,(root)}$	=	Moment of inertia of root fitting about flapping axis due to mass distribution normal to chord plane, slugs ft. <sup>2</sup>
$l$	=	Distance from pitch axis to elastic axis, ft.
$m_{ij}$	=	Generalized mass or inertia coupling coefficient*
$M$	=	Mach number
$m$	=	Mass per unit span, slugs/ft.
$Q$	=	Distance of aerodynamic reference axis aft of pitch axis, ft.
$R$	=	Blade radius, ft.
$r$	=	Spanwise distance from center of rotation, ft.
$r_0$	=	Inboard spanwise limit of integration for aerodynamic forces, ft.
$T_{ij}$	=	Generalized centrifugal force coefficient*
$V_f$	=	Free stream velocity, ft./sec.
$V_T$	=	Tangential velocity of air with respect to blade section = $\Omega r + V_f \sin \psi$ , ft./sec.
$w_o(r)$	=	Downwash velocity at Station $r$ , ft./sec.
$\bar{x}_i$	=	Section c.g. location with respect to the elastic axis (+ aft), ft.
$\bar{x}_E/C$	=	Ratio of equivalent center of gravity position to blade chord = $-\frac{1}{3} \frac{R}{b} \frac{m_{E0}}{m_{00}}$ , positive aft with respect to quarter chord, nondimensional

\* Units determined by equation and term

LIST OF SYMBOLS  
(continued)

$\alpha_T$	=	Angle of tip path plane relative to free stream velocity, rad.
$\Delta\beta$	=	Perturbation flapping angle, rad.
$\beta_0$	=	Initial flapping angle, rad.
$\theta_0$	=	Initial pitch angle, rad. or degrees
$\Delta\theta_0$	=	Perturbation pitching angle, rad.
$\theta_1$	=	Initial blade twist about elastic axis, rad.
$\Delta\theta_1$	=	Perturbation torsional deflection at the blade tip about the elastic axis, rad.
$\mu$	=	Advance ratio, $\frac{V_\infty \cos \alpha_T}{\Omega r}$ nondimensional
$\nu$	=	Ratio of oscillation frequency to shaft rotational speed, nondimensional
$\rho$	=	Air density, slugs/ft. <sup>3</sup>
$\phi(r)$	=	Initial bending deflection at radius r, ft.
$\Delta\phi_n$	=	Perturbation bending displacement at the tip of the blade in n <sup>th</sup> natural mode, ft.
$\psi$	=	Azimuthal angle of blade in rotor disc, zero downwind, rad.
$\Omega$	=	Shaft rotational velocity, rad./sec.
$\omega$	=	Oscillation frequency, rad./sec.
$\omega_i$	=	Uncoupled nonrotating natural frequency of i <sup>th</sup> mode, rad./sec.
$\omega_i$	=	i <sup>th</sup> mode natural frequency at a rotational velocity, $\Omega$ , rad./sec.

## I. INTRODUCTION

The research program discussed herein was undertaken to obtain information on the influence of forward flight speed (advance ratio) on the flutter characteristics of a helicopter rotor blade model. This effort is essentially a continuation of the exploratory program reported in Ref. 1.

The critical flutter speed is a parameter which should be considered by designers in conjunction with forward flight loads. Even if avoided, the combinations of advance ratio and shaft rotational speed at which rotor flutter occurs are important since the magnitude of the response of the blade to normal forward flight aerodynamic excitation is greatly increased as the critical flutter conditions are approached.

The need for a better understanding of the aeroelastic properties of helicopter rotor blades and the need for more accurate means of predicting these properties have been realized for some time. Continuing effort along these lines are demonstrating the close relationships that exist among flutter characteristics, blade aerodynamic loads, blade structural dynamics, vibratory blade stresses, fuselage vibration, blade response to control movement, flight stability, and helicopter performance. Limits of present knowledge prevent the simultaneous evaluation of these problems in the design of helicopter rotor blades. In fact, even the explanations of particular observed phenomena must be qualified with assumptions regarding the interactions of the components of the overall problem unless extreme care has been exercised to isolate only one facet of the rotor dynamic problem.

In recent years, considerable work has been done on the theoretical and experimental study of rotor flutter in hovering flight (e.g., Refs. 2 to 10). These studies were summarized briefly in Ref. 10. At the present time, rotor flutter theory has been developed to the point where fairly good correlation can be expected between theoretical and experimental results for the hovering case. However, comparatively little work has been done to determine the effect of forward velocity on rotor flutter. Reference 11 gives the results of tests of a scale model of a two-bladed, teetering, jet-driven helicopter. In these tests, it was found that the rotor speed at which flutter was first detected decreased slightly as advance ratio was increased from 0 to 0.15. References 12, 13, and 14 discuss the instability of an unconventional jet-driven rotor configuration which employed a floating hub and utilized pitch-cone coupling. For certain ranges of parameters this configuration exhibited a flutter mode in which blade chordwise bending was the dominant degree of freedom. In this case, it was also found that the critical rpm at which flutter occurred decreased with forward speed. The stability of flapping motions

---

Manuscript released by authors, December 1961, for publication as an ASD Technical Report.

was also studied for this configuration. It was shown that a linear mathematical model representing single-degree-of-freedom flapping motions can indicate instability at high advance ratios (Refs. 12 and 13). This characteristic arises from the periodicity of the air velocity relative to the blade as the blade rotates in forward flight.

A pitch-lag-flap instability of a light conventional rotor in hovering was discovered at ASD and subsequently analyzed (Ref. 15). Similar experimental results obtained with a model were reported in Ref. 16 and, in addition, forward flight was found to have a destabilizing effect.

Reference 17 contains the derivation of equations of motion for bending and torsion of a rotor in forward flight - the mechanical terms being the same as those derived in previous analyses for the hovering case (e.g., Refs. 5, 9 and 10). Reversed flow effects were included in the quasi-static aerodynamics. Solutions for first torsion flapping-first bending flutter were obtained by numerical integration of the equations. The shaft rotational speed was fixed during the calculations and the advance ratio was increased until unstable motions were found. Reasonable agreement was shown between two flutter points obtained with models and calculated results at very high advance ratios ( $\mu > 1.0$ ). No calculations or data were presented for flutter at lower advance ratios.

Although the above-mentioned investigations have provided some forward flight flutter data, there is still little information on how forward velocity influences the critical rotor speeds for flutter in the coupled flapping-pitching mode or coupled flapping-pitching-bending-twisting mode of a conventional rotor. Furthermore, no known data exist that cover advance ratios corresponding to the present practical flight regime -  $0 < \mu < 0.4$ . The results of flutter investigations for rotors in hovering flight show that the flutter characteristics depend principally on the effective c.g. position, the generalized mass parameters, the uncoupled natural frequencies of the blade modes, and the collective pitch angle. The trends of the effect of c.g. position, the blade mass, and blade natural frequency (i.e., properties that could be determined in a vacuum) would be expected to be similar in the forward flight case to those found in hovering. Aerodynamic effects, however, are quite different in forward flight due to the cyclic change of the relative tangential velocity at the blade, the unsymmetric induced velocity distribution, and the rotor disk angle of attack. Both the relative tangential velocity and induced velocity effects are functions of the advance ratio parameter and this latter parameter represents the major difference between hovering and forward flight aerodynamics. Also, the rotor disk angle of attack results in a change of the "wake spacing" of elements of shed vorticity due to a change of the transport velocity relative to the plane of the rotor disk.

It was noted in Ref. 11 that the flutter motions occurring in forward flight were not pure sinusoidal motions but were irregular without a well-defined frequency. The irregularity of the motions and stresses is not surprising since they result from the superposition of flutter motions whose frequencies are not necessarily integral multiples of the rpm on the normal forced response in forward flight.

Theoretical investigations have been made of combined flapping and bending instability of a rotor blade in forward flight (Ref. 18). Instability at high advance ratios ( $\mu > 1$ ) was shown to be possible for the mathematical model chosen. It is reasonable to expect that this instability would be more critical if adversely coupled with blade pitching or torsional motions.

It is evident from the above review that little data existed on the effects of translational velocity on helicopter rotor blade flutter characteristics prior to the experimental phase of the Ref. 1 program and that few theoretical analyses of the problem had been made. In particular, no experimental or theoretical results were available in the practical helicopter range ( $0.15 \leq \mu \leq 0.4$ ). The present program is essentially a continuation of the work reported in Ref. 1. Techniques and equipment employed were substantially the same. Discussion of these is incorporated in this report for the convenience of the reader.

Blade chordwise center-of-gravity position, collective pitch angle, and pitching natural frequency as well as advance ratio were varied during the flutter tests.

These same quantities (except collective pitch angle) were also varied in the theoretical calculations. Effects of reverse flow were incorporated in the aerodynamic force expressions and their influence on the theoretical flutter boundaries was determined.

## II. TEST APPARATUS

The test equipment used in the present program consisted of a single-bladed hydraulically-driven rotor mounted on the tower of the Small Rotorcraft Test Apparatus (Figs. 1a and 1b). This same equipment was used to obtain the experimental results reported in Ref. 1.

The Small Rotorcraft Test Apparatus (Ref. 19) was built by CAL under the sponsorship of the Army Aviation Division of the U. S. Army Transportation Research and Engineering Command for making force measurements on small craft or models at low speeds. Mounted under the trailer is a 375-hp engine for driving the model or machine being tested (Fig. 2). Two 110-volt 60 cycle gasoline-driven generators, one having 1500 watts and the other 3500 watts output capacity, are mounted under the floor of the trailer. A hydraulic pump to operate the pitch strut and the tower extension strut is mounted under the trailer bed. During the present program, the trailer tower was used in its lowest position, and the pitch angle of the pylon was varied. Figure 3 shows the tractor used to pull the trailer. The test conductor sits in the tractor facing aft, and from this position he can observe the model and operate its controls.

The rotor head (Fig. 4) had been used during previous programs to obtain the flutter data in hovering reported in Refs. 4, 6, 7, 9 and 10. The blade had been flutter tested previously in hovering (Ref. 10). A motor-driven cam was used to disturb the blade in pitch. This device had also been used in previous tests (Refs. 4 and 6).

The rotor is mounted on a drive shaft that is supported by bearings at each end of the rotor pylon (Figs. 1a and 1b). A slip ring assembly is mounted on the drive shaft under the lower bearing. The rotor drive shaft is driven through a flexible coupling by a 29-hp hydraulic motor. The hydraulic motor housing is supported by trunnion bearings on the top of the tower of the Small Rotorcraft Test Trailer. A hydraulic strut pinned to the hydraulic motor housing and the tower is used to change the pitch angle of the pylon (Fig. 1a).

Hydraulic power to drive the motor that is connected to the rotor drive shaft was obtained by mounting a hydraulic pump at the base of the trailer tower and driving it with the 375-hp engine (Fig. 5). The speed of the hydraulic motor can be controlled by varying the stroke of the pump or by changing the speed of the driving engine.

The blade used to obtain the flutter data is designated as Blade No. 4, in Ref. 10. Its properties are tabulated in APPENDIX I of this report. Blade chordwise center-of-gravity position was adjusted by means of lead weights

housed in a cylindrical pod at the blade tip. The blade is instrumented with strain gages to measure bending moments at five spanwise locations. Pitch and flap transducers are mounted on the rotor (Fig. 4). The signals from this instrumentation are carried through the slip rings to a recording oscillograph that is mounted on the trailer (Fig. 6). The hydraulic controls for operating the tower extension and pylon pitch struts are also shown on Fig. 6.

### III. FLUTTER EXPERIMENTS

#### A. Technique

The same technique and pitch trip actuator had been used previously in model flutter studies (Refs. 1, 4, and 6) and, therefore, are described only briefly in the following discussion.

In order to excite the model and subsequently determine the proximity to the flutter boundary, the pitch of the blade was increased several degrees above the nominal value by means of a motor-driven cam and then suddenly released. The motions of the blade would damp out if the model were rotating with an angular velocity below that required to sustain flutter. Rotor speed was increased in increments and the process repeated until the angular velocity of the rotor was a small amount greater than that at which blade motions damped out, and the blade motions persisted at almost constant amplitude. The oscillograph was started, and rotor speed was slowly decreased until flutter motions damped out. The conditions existing just before the motion started to decay were considered to be the flutter conditions.

Since the purpose of this investigation was to study the effect of forward velocity on the flutter of a single-bladed rotor, tests were first made with zero or near zero forward velocity to establish a reference flutter condition.

Flutter tests were conducted at the Niagara Falls Municipal Airport on the East-West taxi strip. The velocity and direction of the ambient wind limited the lowest forward flight speed at which tests could be conducted. Tests were not attempted unless the angle between the resultant wind velocity and the plane of symmetry of the model was less than fifteen degrees. This arbitrary limit was set to avoid the introduction of an additional test variable-lateral shaft tilt. Runs were made with the model faced into the prevailing wind and with the apparatus stationary to obtain the lower range of test forward flight velocities.

#### B. Range of Experiments

Tests were conducted for a range of equivalent center-of-gravity locations\* from 0.36 to 13.9 percent chord behind the pitch axis. The pitch axis was at the 25% chord line.

\* Equivalent center-of-gravity location is a convenient means for presenting the blade pitching-flapping inertial coupling - i.e., the product of inertia. It is defined as the chordwise c.g. location of a rectangular blade having a uniform mass distribution such that the ratio of the pitching-flapping product of inertia to the flapping inertia is the same as that of the non-uniform blade being studied:

$$\frac{\bar{x}_E}{C} = -\frac{1}{3} \frac{R}{b} \frac{M_{\theta\theta}}{M_{\phi\phi}}$$

## B. Range of Experiments (cont'd)

The advance ratio range was zero to approximately 0.7. Flutter tests were conducted for shaft angles between 4 and 12 degrees. Collective pitch angles ranged from 3 to 8 degrees.

The ratio of the nonrotating bending frequency to the nonrotating pitching frequency could be varied from 0.6 to 1.5. The primary means for varying this quantity was the spring stiffness of the pitching mode.

Approximate stall regions were computed for the retreating blade tip and are shown on Fig. 7 as functions of shaft tilt angle,  $\alpha$ , and collective pitch angle,  $\theta_0$ . It was assumed that the stall angles of attack are  $+14^\circ$ . Linear aerodynamic theory was used to calculate the conditions at which these aerodynamic angles of attack were reached. The regions between the lines  $\mu = \text{constant}$  represent unstalled operation. The model blade tip was unstalled in the trim condition for all the data presented and it is doubtful that any local stalling due to the flutter motions affected the results.

## C. Experimental Flutter Results

The experimental flutter data are summarized on Figs. 8a - 8e. The various shaft tilts (from  $4^\circ$  to  $12^\circ$  nose-down tilt relative to the wind) at which data were obtained are not shown on the figures since the effect of this parameter was hidden in the scatter of the flutter points.

Data obtained with blade nearly mass balanced (equivalent c.g. 0.36% chord behind the quarter chord) are shown on Fig. 8a. The ratio of the nonrotating pitching frequency,  $\omega_p$ , to the shaft speed,  $\Omega$ , at which flutter occurred was insensitive to shaft tilt, advance ratio, and bending-to-pitching frequency ratio over the range tested.

Figure 8b shows the flutter data obtained with the equivalent c.g. approximately 4% chord behind the pitch axis (25% chord). The shaft speeds at which flutter occurred for a given pitching frequency were reduced compared with those for the more forward c.g. location (Fig. 8a). Again, advance ratio and shaft angle and bending-to-pitching ratio had small effects on the flutter characteristics.

Flutter points obtained with equivalent c.g. approximately 6% behind the quarter chord are shown on Figs. 8c and 8d. The data obtained at relatively low collective pitch angles (Fig. 8c) indicate a decreasing flutter speed ( $\Omega$ ) with increasing advance ratio for a fixed pitching frequency. Shaft tilt and frequency ratio again had relatively small effects. Figure 8d shows results obtained at somewhat higher collective pitch angles. Comparison of Figs. 8c and 8d indicates that the higher collective pitch angles produced lower flutter speeds in the low  $\Omega$  range while practically no difference

assignable to collective pitch can be observed for  $\mu > 0.3$ .

Test results for the most aft c.g. location (approximately 14% behind the pitch axis) are shown on Fig. 8e. Both advance ratio and bending-to-pitching frequency ratio had appreciable effects.

#### IV. DISCUSSION OF ANALYSES

##### A. Equations of Motion

The method of derivation of the equations of motion used in the present program follows that used in the previous CAL studies of blade aeroelastic characteristics (e.g., Refs. 1, 5, 7, 9, and 10). The mass and elastic terms are not rederived in this report, since these terms are identical in hovering and forward flight. Similarly, the quasi-static aerodynamic terms arising from the translational velocity were previously presented in Ref. 1 (with reversed flow effects neglected) and are easily derived by an extension of the basic analysis of Ref. 6. The equations of motion and the expressions for the generalized mass, elastic, and aerodynamic coefficients are summarized in APPENDIX II. A correction factor to approximate the principal Mach number effect (i. e., on the lift curve slope) has been indicated. The inclusion of even this simple factor and the effects of reversed flow over the retreating blade greatly complicates the problem. Mach number effects were not included in the calculations made for the blade used in the present program, since the Mach numbers reached during the tests were low ( $M < 0.3$ ).

It must be noted that there is no substantiated theory for the prediction of either the steady or unsteady aerodynamic forces on a helicopter rotor blade in forward flight.

##### B. Aerodynamic Coefficients for Reversed Flow Region

A helicopter rotor blade in forward flight experiences a periodic tangential velocity arising from the flight speed superimposed on the tangential velocity due to rotation:

$$V_T = \Omega r + V_f \sin \psi$$

where the azimuthal angle,  $\psi$ , is measured from the downwind position and the positive direction is the direction of rotation of the blade. When  $V_T < 0$  the flow regime is termed "reversed".

The boundary at which  $V_T = 0$  is a circle of diameter  $\mu R$  with its center at  $\psi = \frac{3\pi}{2}$ ,  $r = \frac{1}{2}\mu R$ . Within this circle, the lift is

negative and the static aerodynamic center is at the  $3/4$  chord of the blade section.

In order to extend the theory developed in Refs. 1 and 6 to account for the reversed flow effect, a correction factor was added to the sectional aerodynamic lift equation. This factor subtracts the portion of the lift due to

normal flow and adds terms due to reversed flow. Let the lift be considered to consist of two parts:

$$P = P_{NF} + \Delta P_{RF} \quad (1)$$

where

$$\begin{aligned} P &= \text{resultant lift} \\ P_{NF} &= \text{lift in the absence of reversed flow} \\ \Delta P_{RF} &= \text{lift correction due to reversed flow} \end{aligned}$$

then

$$\Delta P_{RF} = -P_{NF} + P \quad (2)$$

It is understood, of course, that this correction is applied only in the region  $V_T < 0$ .

Identification of the terms in the lift equation that are affected by the reversed flow regions was accomplished by writing the lift equation for reversed flow and comparing it with the expression obtained when  $V_T > 0$ . This is substantially the same procedure used in Ref. 17. For  $V_T > 0$ , the lift equation is

$$P = \pi \rho b^2 [\dot{v} \alpha + \dot{h}] + a \rho b v [\dot{v} \alpha + \dot{h} + \frac{1}{2} b \dot{\alpha}] \quad (3)$$

For  $V_T < 0$  ( i.e., reversed flow region),

$$P = \pi \rho b^2 [\dot{v} \alpha + \dot{h}] + a_{RF} \rho b v [-\dot{v} \alpha - \dot{h} + \frac{1}{2} b \dot{\alpha}] \quad (4)$$

It is seen that the signs of the  $\dot{v} \alpha$  and  $\dot{h}$  terms became negative in the reverse flow lift equation. By identifying these terms in the theory (Refs. 7 and 17), the equation for the perturbation lift of a blade element operating in reverse flow and correction terms indicated by Equation (2) was obtained. By means of the same procedure, it was found that for a flat plate airfoil there are no changes in the signs of the terms in the equation expressing the moment about the mid-chord of the blade.

The correction terms appear as integrals over the interval  $\tau$  to  $\sin$  in APPENDIX II. Evaluation of the integrals leads to periodic force expressions since the upper limit is periodic.

When (at an element of the blade)  $V_f \sin \psi \approx \Omega r$  i.e.,  $V_T \approx 0$ , the angle-of-attack of the blade may be considerably larger than the stall angle and the blade lift will be reduced. The lift curve slope was carried in the reversed flow aerodynamic coefficients as a parameter in order to permit study of this nonlinear effect at some future time.

### C. Flutter Calculations

The equations of motion for flapping, pitching and bending given in APPENDIX II were programmed on an analog computer. In order to reduce the problem to a size which was compatible with the available computer facilities, the following engineering approximations to the problem were made.

- a. The effects of the blade torsional degree-of-freedom were neglected.
- b. The effects of aerodynamic coupling between the blade flapping and bending were neglected in the reverse flow terms.
- c. The effects of terms of higher harmonic order than 4 (e.g.,  $\cos 5\psi$ ,  $\sin 5\psi$ , etc.) in the terms describing reverse flow were neglected.

It is believed that the accuracy with which the flutter boundaries for the model blade are predicted is not significantly altered by these approximations when the advance ratio is that characteristic of foreseeable helicopters (say,  $\mu < 0.7$ ).

Reversed flow aerodynamic terms for the bending generalized coordinate were generated by using an approximate mode shape (cubic). This procedure permitted closed form integration and greatly simplified the introduction of the upper limit,  $\mu \sin \psi$  (see APPENDIX II).

Since the blade encounters reverse flow only on the retreating blade, it is necessary to switch the reverse flow terms into the equations of motion when  $\pi < \psi < 2\pi$  and out when  $0 < \psi < \pi$ . This was accomplished by the use of electrical relays in the analog computations.

The solutions obtained on the analog computer are presented on Figs. 9a through 9i. The ordinate,  $\bar{\omega}_q / \Omega$ , is directly proportional to  $1/\Omega$  for a fixed nonrotating pitch frequency. Hence, increasing values of the ratio correspond to decreasing flutter speeds,  $\Omega$ , when the pitching frequency,  $\bar{\omega}_p$ , is specified. For each of the three center-of-gravity positions studied the effects of bending-to-pitching frequency ratio and reversed flow were obtained.

Calculated results for the most forward equivalent center-of-gravity position ( $\bar{x}_E/c = 0.0036$  behind the pitch axis) are shown on Figs. 9a through 9c. Curve A on Fig. 9a was obtained with reversed flow effects neglected; Curve B was obtained by using the assumption that the forces generated in the reversed flow region were zero, and curve C was obtained when linear aerodynamic theory (see Section IVA) was used to represent the reversed flow aerodynamic forces. It can be seen that the effect of including reversed flow terms in the computation is to reduce the shaft rotational speed at which flutter is predicted. For this particular case reduction is relatively small until an advance ratio of 0.65 is reached. Both with and without reversed flow the calculated flutter speed at  $\mu = 0.4$  was approximately 15% lower than that at  $\mu = 0.2$ .

Comparison of Figs. 9a, 9b, and 9c indicates the effect of the ratio of the nonrotating bending frequency to the nonrotating pitching frequency. The lowest frequency ratio ( $\bar{\omega}_\phi/\bar{\omega}_\theta = 0.585$ , Fig. 9c) indicated the lowest flutter speed in the low  $\mu$  range. For this particular case the bending frequency is near the flapping frequency (the rotating flapping frequency ratio being constant and equal to one, of course). Effects of reversed flow and advance ratio are roughly the same for all these frequency ratios.

The peculiar shapes of the curves on Figs. 9a, 9b, and 9c indicate that the aerodynamic terms introduce complex phase shifts that are functions of advance ratio.

Figures 9d through 9f show the calculated results for an intermediate center-of-gravity position ( $\bar{x}_E/c = 0.044$ ) for three bending-to-pitching frequency ratios. Effects of reversed flow were relatively minor up to an advance ratio of approximately 0.5. Distortion of the theoretical curves occurred as  $\bar{\omega}_\phi/\bar{\omega}_\theta$  was decreased. An appreciable decrease of the flutter speed was obtained at  $\mu = 0.6$  for  $\bar{\omega}_\phi/\bar{\omega}_\theta = 0.947$  when reversed flow effects were included (Fig. 9e). Figure 9d, on the other hand, indicated that flutter speeds in the range  $0.3 < \mu < 0.5$  for  $\bar{\omega}_\phi/\bar{\omega}_\theta = 0.583$  were higher than the flutter speed at  $\mu = 0.3$ .

Results obtained with the center of gravity most aft ( $\bar{x}_E/c = 0.139$ ) show the most sensitivity to  $\bar{\omega}_\phi/\bar{\omega}_\theta$  and advance ratio (Figs. 9g through 9i). Figure 9g again shows a comparison between the results obtained with different assumptions with respect to the aerodynamic forces in the reversed flow region. Neglect of reversed flow usually gives the highest value of the shaft speed at which flutter occurs. Results obtained by assuming the aerodynamic forces in the reversed flow region are zero indicate a lower flutter speed while inclusion of fully effective reversed flow aerodynamic forces yields the lowest values of  $\Omega$ .

For  $\bar{u}_p/\bar{u}_e = 1.55$  (Fig. 9g) and 0.629 (Fig. 9i) the theoretical curves indicate a rapid decrease of flutter speed with advance ratio. For  $\bar{u}_p/\bar{u}_e = 1.11$

the decrease of flutter speed with increasing advance ratio is less pronounced (Fig. 9h) -- in fact, the trend is reversed in a narrow range at an advance ratio of approximately 0.5. Both Figs. 9h and 9i indicate some conditions for which the blade is slightly more stable with reversed flow effects included than with reversed flow neglected.

## V COMPARISON OF EXPERIMENTAL AND CALCULATED RESULTS

Comparisons of experimental and calculated flutter boundaries are shown on Figures 10a through 10c. In general, the calculated results are conservative, i.e., the predicted shaft speed for flutter is lower than that observed in the tests.

A comparison of the results obtained with the blade nearly mass-balanced is shown in Figure 10a. This plot is a combination of Figures 8a, 9a and 9b. Predicted degradation of the aeroelastic stability with advance ratio was not observed--at least over the range of advance ratios investigated. The calculated flutter boundary is conservative even when reversed flow effects are neglected.

Figure 10b presents a comparison of the measured and calculated flutter boundaries for an intermediate c.g. location,  $\bar{x}_e/c = 0.04$ . Again, the experimental data show no sensitivity to advance ratio while the theoretical results indicate a decreasing flutter speed with increasing advance ratio. The theoretical results are quite conservative over the range covered by tests.

Experimental and theoretical results for  $\bar{x}_e/c = 0.139$  are shown on Figure 10c. The experimental data show a decreasing flutter speed with increasing advance ratio similar to that obtained in the theoretical study. The calculated results are conservative over the range of the test data.

## VI CONCLUSIONS

1. Advance ratio had little effect on the shaft speed at which flutter was obtained experimentally when the blade was nearly mass-balanced--at least, up to an advance ratio of approximately 0.5. As the mass unbalance was increased, the flutter speed became more sensitive to advance ratio and decreased with increasing advance ratio. The same trends were observed in the theoretical results, but the agreement is only qualitative.
2. Bending-to-pitching frequency ratio had little effect on observed flutter speed for the range of conditions tested ( $0.6 < \bar{\omega}_y / \bar{\omega}_\theta < 1.5$ ). Whatever effect existed was obscured in the scatter of the data. Theoretical results showed a sensitivity to this ratio that varied with unbalance and advance ratio.
3. The theoretical results were conservative for all combinations of unbalance, bending-to-pitching frequency ratio, and advance ratio encompassed by the test data.
4. Collective pitch angle had an observable effect on the experimental flutter speed at low advance ratios, but this effect disappeared at moderate advance ratios ( $\mu > 0.2$ ). It is possible that blade stall partly influenced the experimental observations, since the amplitudes of the pitch motions were relatively large. Collective pitch effects were neglected in the analysis, since the quasi-steady aerodynamic theory used indicated these are second-order effects.
5. It is difficult to define experimentally a flutter boundary as a function of advance ratio, because the flutter motions are superimposed on the forced response motions.
6. The calculated effect of reversed flow was to decrease the shaft speed at which flutter occurred for nearly all blade configurations. The magnitude of this effect varied with advance ratio, bending-to-pitching frequency, and blade unbalance. Inclusion of reversed flow effects did not improve the agreement between the experimental and theoretical results. That is, the theoretical boundary was conservative even when reversed flow effects were neglected.
7. Extreme caution should be exercised in the extrapolation of the experimental results obtained to rotors having mass, elastic, and geometric properties appreciably different from the test configurations.

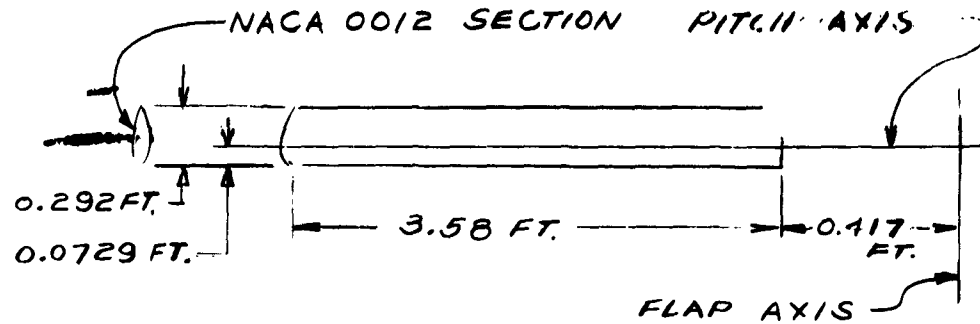
## VII RECOMMENDATIONS

The scope of this investigation was so limited that many potentially important problems were not attacked. Some of these are contained in the following list:

1. An unsteady aerodynamic theory should be developed for rotors in forward flight.
2. An experimental and theoretical investigation of the effects of Mach number on rotor flutter should be conducted.
3. Means for predicting contours of constant damping (as opposed to the contours of zero net damping--the flutter boundary) should be developed and substantiated.
4. Stall flutter should be investigated.
5. A theoretical and experimental study of the aeroelastic characteristics of VTOL/STOL rotor-props should be initiated.
6. Aeroelastic studies of unloaded rotors operating at very high advance ratios ( $\mu > 1$ ) should be undertaken.

## APPENDIX I

### MODEL PHYSICAL CHARACTERISTICS



### BLADE PLAN-VIEW DIMENSIONS

The above diagram shows the plan-view dimensions of CAL Model Blade 4. The properties of the blade and hub are summarized in the following tables:

Table I.1	Section Mass and Stiffness Properties for CAL Model Blade 4.
Table I.2	Blade and Hub Properties
Table I.3	Hub Inertial Characteristics.

TABLE I.1  
SECTION MASS AND STIFFNESS PROPERTIES FOR CAL MODEL BLADE L<sub>1</sub>

Section Number	Spanwise c.g., ft.	Flapwise Bending Stiffness (EI) <sub>2</sub> , lb.-in. <sup>2</sup>	Mass of Section, Slugs	Chordwise c.g. (+ aft C/L), ft.	Pitching Inertia Relative to Elastic Axis, slugs ft. <sup>2</sup>	Torsional Stiffness (GJ) <sub>2</sub> , lb.-in.
1	4.000	14,850	0.000000			
2	3.958	14,850	0.001348	0.04924	0.7825 x 10 <sup>-5</sup>	12,250
3	3.708	14,850	0.001585	0.05298	1.058 x 10 <sup>-5</sup>	12,250
4	3.458	14,850	0.001876	0.05049	1.131 x 10 <sup>-5</sup>	12,250
5	3.208	14,850	0.001585	0.05298	1.058 x 10 <sup>-5</sup>	12,250
6	2.958	14,850	0.001876	0.05049	1.131 x 10 <sup>-5</sup>	12,250
7	2.708	14,850	0.001585	0.05298	1.058 x 10 <sup>-5</sup>	12,250
8	2.458	14,850	0.001876	0.05049	1.131 x 10 <sup>-5</sup>	12,250
9	2.208	14,850	0.001585	0.05298	1.058 x 10 <sup>-5</sup>	12,250
10	1.958	14,850	0.001876	0.05049	1.131 x 10 <sup>-5</sup>	12,250
11	1.708	14,850	0.001585	0.05298	1.058 x 10 <sup>-5</sup>	12,250
12	1.458	14,850	0.001585	0.05298	1.058 x 10 <sup>-5</sup>	12,250
13	1.208	14,850	0.001585	0.05298	1.058 x 10 <sup>-5</sup>	12,250
14	.958	20,000	0.001589	0.05155	1.050 x 10 <sup>-5</sup>	12,250
15	.708	130,000	0.003763	0.02943	1.612 x 10 <sup>-5</sup>	12,250
16	.500	--	0.003607	0.01962	1.205 x 10 <sup>-5</sup>	--
HUB			See Table I.3 for Hub Inertia			

TABLE I.2  
BLADE AND HUB PROPERTIES -- CAL BLADE MODEL 4 -- NO POD

<u>ITEM</u>	<u>VALUE</u>
Elastic Axis Location (Uniform Part of Blade)	41.0% chord
C.G. Position (Uniform Part of Blade)	42.5% chord
$m_{\beta\beta}$ . . . . .	0.187 slugs ft. <sup>2</sup>
$m_{\theta\theta}^*$ . . . . .	0.00038 slugs ft. <sup>2</sup>
$m_{\phi\phi}$ . . . . .	0.0103 slugs
$m_{\theta\theta}$ . . . . .	0.00006 slugs ft. <sup>2</sup>
$m_{\beta\theta} = m_{\theta\beta}$ . . . . .	-0.0028 slugs ft. <sup>2</sup>
$m_{\beta\phi} = m_{\phi\beta}$ . . . . .	-0.00044 slugs ft.
$m_{\beta\theta} = m_{\theta\beta}$ . . . . .	-0.00017 slugs ft. <sup>2</sup>
$m_{\theta\phi} = m_{\phi\theta}$ . . . . .	-0.00007 slugs ft.
$m_{\phi\phi}$ . . . . .	0.00008 slugs ft. <sup>2</sup>
$m_{\phi\theta} = m_{\theta\phi}$ . . . . .	-0.00002 slugs ft.
$I_z^*$ . . . . .	0.000073 slugs ft. <sup>2</sup>

---

\*Includes blade and part of hub that pitches.

TABLE I.3  
HUB INERTIAL CHARACTERISTICS

$\Delta I_r$	=	0.0341 slugs ft. <sup>2</sup>	(all parts that flap)
$I_{zf}$	=	0.00205 slugs ft. <sup>2</sup>	(part that flaps but does not pitch)
$\Delta I_x,$	=	0.000094 slugs ft. <sup>2</sup>	(part that pitches)
$I_{z,}$	=	0.000073 slugs ft. <sup>2</sup>	(part that pitches)
$I_{z,} \text{ (root)}$	=	$I_{zf} + I_{z,}$	= 0.00212 (slugs ft. <sup>2</sup> )

## APPENDIX II

### EQUATIONS OF MOTION AND GENERALIZED COEFFICIENTS

This appendix contains the equations for the pitching, flapping, bending and torsion degrees of freedom and the expressions for the coefficients. These are arranged in the following tables:

Table II.1	-	Equations of Motion
II.2	-	Generalized Mass Coefficients
II.3	-	Generalized Centrifugal Force Coefficients
II.4	-	Generalized Gyroscopic Coupling Coefficients
II.5	-	Generalized Aerodynamic Coefficients

The preceding were derived in a manner similar to that described in Reference 7. Underlined terms in Tables II.2, II.3, and II.4 are functions of the static deflections of the blade.

The lift curve slope appears under the integral signs in Table II.5 to indicate that it is a function of radial (and azimuthal) position when the Mach number effect is included. It is anticipated that the Prandtl-Glauert correction will be suitable for the range of section Mach numbers anticipated for helicopter rotors (Reference 20):  $a = a_{M=0} / \sqrt{1 - M^2}$

## EQUATIONS OF MOTION

$$\begin{aligned}
& [m_{\alpha} - A_{\alpha}] \Delta \phi - [\Omega \varepsilon G_{\alpha} + A_{\alpha} + S_{\alpha} \mu \sin \gamma] \Delta \phi + [\Omega^2 \left( \frac{\omega^2}{\Omega^2} m_{\alpha} - T_{\alpha} \right) - A_{\alpha} - C_{\alpha} \mu \cos \gamma - S_{\alpha} \mu \sin \gamma - S'_{\alpha} \mu' \sin 2\gamma] \Delta \phi \\
& + [m_{\alpha} - A_{\alpha}] \Delta \theta - [\Omega \varepsilon G_{\alpha} + A_{\alpha} + S_{\alpha} \mu \sin \gamma] \Delta \theta + [\Omega^2 \left( \frac{K_{\alpha}}{\Omega^2} - T_{\alpha} \right) - A_{\alpha} + C'_{\alpha} \mu' - S_{\alpha} \mu \sin \gamma - C'_{\alpha} \mu' \cos 2\gamma] \Delta \theta \\
& + [m_{\beta} - A_{\beta}] \Delta \phi - [\Omega \varepsilon G_{\beta} + A_{\beta} + S_{\beta} \mu \sin \gamma] \Delta \phi + [\Omega^2 \left( \frac{K_{\beta}}{\Omega^2} - T_{\beta} \right) - A_{\beta} - C_{\beta} \mu \cos \gamma - S_{\beta} \mu \sin \gamma - S'_{\beta} \mu' \sin 2\gamma] \Delta \phi \\
& + [m_{\beta} - A_{\beta}] \Delta \theta - [\Omega \varepsilon G_{\beta} + A_{\beta} + S_{\beta} \mu \sin \gamma] \Delta \theta + [\Omega^2 \left( \frac{K_{\beta}}{\Omega^2} - T_{\beta} \right) - A_{\beta} + C'_{\beta} \mu' - S_{\beta} \mu \sin \gamma - C'_{\beta} \mu' \cos 2\gamma] \Delta \theta = 0 \quad (1)
\end{aligned}$$

$$\begin{aligned} & [m_{\alpha\beta} - A_{\alpha\beta}]d\dot{\varphi} - [\Omega \varepsilon G_{\alpha\beta} + A_{\alpha\beta} + S_{\alpha\beta} \mu \sin \varphi]d\dot{\varphi} + [\Omega^2 \left( \frac{K_{\alpha\beta}}{\Omega^2} - T_{\alpha\beta} \right) A_{\alpha\beta} - C_{\alpha\beta} \mu \cos \varphi - S_{\alpha\beta} \mu \sin \varphi - S'_{\alpha\beta} \mu^2 \sin 2\varphi]d\varphi \\ & + [m_{\alpha\beta} - A_{\alpha\beta}]d\dot{\varphi} - [\Omega \varepsilon G_{\alpha\beta} + A_{\alpha\beta} + S_{\alpha\beta} \mu \sin \varphi]d\dot{\varphi} + [\Omega^2 \left( \frac{K_{\alpha\beta}}{\Omega^2} m_{\alpha\beta} - T_{\alpha\beta} \right) A_{\alpha\beta} + C'_{\alpha\beta} \mu^2 - S_{\alpha\beta} \mu \sin \varphi - C'_{\alpha\beta} \mu^2 \cos 2\varphi]d\varphi \\ & + [m_{\alpha\beta} - A_{\alpha\beta}]d\dot{\varphi} - [\Omega \varepsilon G_{\alpha\beta} + A_{\alpha\beta} + S_{\alpha\beta} \mu \sin \varphi]d\dot{\varphi} + [\Omega^2 \left( \frac{K_{\alpha\beta}}{\Omega^2} - T_{\alpha\beta} \right) A_{\alpha\beta} - C_{\alpha\beta} \mu \cos \varphi - S_{\alpha\beta} \mu \sin \varphi - S'_{\alpha\beta} \mu^2 \sin 2\varphi]d\varphi \\ & + [m_{\alpha\beta} - A_{\alpha\beta}]d\dot{\varphi} - [\Omega \varepsilon G_{\alpha\beta} + A_{\alpha\beta} + S_{\alpha\beta} \mu \sin \varphi]d\dot{\varphi} + [\Omega^2 \left( \frac{K_{\alpha\beta}}{\Omega^2} - T_{\alpha\beta} \right) A_{\alpha\beta} + C'_{\alpha\beta} \mu^2 - S_{\alpha\beta} \mu \sin \varphi - C'_{\alpha\beta} \mu^2 \cos 2\varphi]d\varphi = 0 \quad (2) \end{aligned}$$

$$\begin{aligned} & [m_{\mu\nu} - A_{\mu\nu}] \Delta \phi - [\Omega_2 G_{\mu\nu} + A_{\mu\nu} + S_{\mu\nu} \mu \sin \psi] \Delta \phi + [\Omega^2 \left( \frac{K_{\mu\nu}}{H^2} - T_{\mu\nu} \right) - A_{\mu\nu} - C_{\mu\nu} \mu \cos \psi - S_{\mu\nu} \mu \sin \psi - S'_{\mu\nu} \mu' \sin 2\psi] \Delta \phi \\ & + [m_{\mu\alpha} - A_{\mu\alpha}] \Delta \alpha - [\Omega_2 G_{\mu\alpha} + A_{\mu\alpha} + S_{\mu\alpha} \mu \sin \psi] \Delta \alpha + [\Omega^2 \left( \frac{K_{\mu\alpha}}{H^2} - T_{\mu\alpha} \right) - A_{\mu\alpha} + C'_{\mu\alpha} \mu' - S_{\mu\alpha} \mu \sin \psi - C'_{\mu\alpha} \mu' \cos 2\psi] \Delta \alpha \\ & + [m_{\nu\beta} - A_{\nu\beta}] \Delta \beta - [\Omega_2 G_{\nu\beta} + A_{\nu\beta} + S_{\nu\beta} \mu \sin \psi] \Delta \beta + [\Omega^2 \left( \frac{K_{\nu\beta}}{H^2} - T_{\nu\beta} \right) - A_{\nu\beta} - C_{\nu\beta} \mu \cos \psi - S_{\nu\beta} \mu \sin \psi - S'_{\nu\beta} \mu' \sin 2\psi] \Delta \beta \\ & + [m_{\nu\alpha} - A_{\nu\alpha}] \Delta \alpha - [\Omega_2 G_{\nu\alpha} + A_{\nu\alpha} + S_{\nu\alpha} \mu \sin \psi] \Delta \alpha + [\Omega^2 \left( \frac{K_{\nu\alpha}}{H^2} - T_{\nu\alpha} \right) - A_{\nu\alpha} + C'_{\nu\alpha} \mu' - S_{\nu\alpha} \mu \sin \psi - C'_{\nu\alpha} \mu' \cos 2\psi] \Delta \alpha = 0 \quad (3) \end{aligned}$$

$$\begin{aligned}
& [m_{\alpha\beta} - A_{\alpha\beta}] \Delta\phi - [\Omega^2 G_{\alpha\beta} + A_{\alpha\beta} + S_{\alpha\beta\mu} \sin \varphi] \Delta\phi + [\Omega^2 (\frac{K_{\alpha\beta}}{\Omega^2} - T_{\alpha\beta} - A_{\alpha\beta} - C_{\alpha\beta\mu} \cos \varphi - S_{\alpha\beta\mu} \sin \varphi - S'_{\alpha\beta\mu} \sin 2\varphi) \Delta\phi \\
& + [m_{\alpha\alpha} - A_{\alpha\alpha}] \Delta\phi - [\Omega^2 G_{\alpha\alpha} + A_{\alpha\alpha} + S_{\alpha\beta\mu} \sin \varphi] \Delta\phi + [\Omega^2 (\frac{K_{\alpha\alpha}}{\Omega^2} - T_{\alpha\alpha} - A_{\alpha\alpha} + C'_{\alpha\beta\mu} - S_{\alpha\beta\mu} \sin \varphi - C'_{\alpha\beta\mu} \cos 2\varphi) \Delta\phi \\
& + [m_{\beta\beta} - A_{\beta\beta}] \Delta\phi - [\Omega^2 G_{\beta\beta} + A_{\beta\beta} + S_{\beta\mu} \sin \varphi] \Delta\phi + [\Omega^2 (\frac{K_{\beta\beta}}{\Omega^2} - T_{\beta\beta} - A_{\beta\beta} - C_{\beta\mu} \cos \varphi - S_{\beta\mu} \sin \varphi - S'_{\beta\mu} \sin 2\varphi) \Delta\phi \\
& + [m_{\beta\alpha} - A_{\beta\alpha}] \Delta\phi - [\Omega^2 G_{\beta\alpha} + A_{\beta\alpha} + S_{\beta\mu} \sin \varphi] \Delta\phi + [\Omega^2 (\frac{\omega^2 m_{\beta\alpha}}{\Omega^2} - T_{\beta\alpha} - A_{\beta\alpha} + C'_{\alpha\beta\mu} - S_{\beta\mu} \sin \varphi - C'_{\alpha\beta\mu} \cos 2\varphi) \Delta\phi = 0 \quad (4)
\end{aligned}$$

TABLE II.2

## GENERALIZED MASS COEFFICIENTS

$$M_{\rho\rho} = I_r + I_z, (\text{root})$$

$$M_{\rho e} = -\int_0^R (1 + \bar{x}_1 + \phi e_0) r m dr$$

$$M_{\rho\phi_n} = \int_0^R f_{\phi_n} r m dr = 0$$

$$M_{\rho e_1} = -\int_0^R \bar{x}_1 r f_{e_1} m dr$$

$$M_{e\rho} = M_{\rho e}$$

$$M_{e e} = I_{x_1} + I_{z_1} + \int_0^R (1 + e \bar{x}_1) m dr + \int_0^R \phi^2 m dr$$

$$M_{e\phi_n} = -\int_0^R f_{\phi_n} (1 + \bar{x}_1 + \phi e_0) m dr + \int_0^R f_{\phi_n}^* \phi e_0 m dr$$

$$M_{e e_1} = \int_0^R \left( \frac{dI_{x_1}}{dr} + \frac{dI_{z_1}}{dr} \right) f_{e_1} dr + \int_0^R \bar{x}_1 e f_{e_1} m dr$$

$$M_{\phi_n\rho} = M_{\rho\phi_n}$$

$$M_{\phi_n e} = M_{e\phi_n}$$

$$M_{\phi_n\phi_n} = \int_0^R f_{\phi_n}^2 m dr + \left( \frac{d f_{\phi_n}}{dr} \right)_{r=0}^2 I_{z_1}(\text{root})$$

$$M_{\phi_n e_1} = -\int_0^R \bar{x}_1 f_{\phi_n} f_{e_1} m dr$$

$$M_{e\rho} = M_{\rho e}$$

$$M_{e e_0} = M_{e_0 e}$$

$$M_{e\phi_n} = M_{\phi_n e}$$

$$M_{e e_1} = \int_0^R \left( \frac{dI_{x_1}}{dr} + \frac{dI_{z_1}}{dr} \right) f_{e_1}^2 dr$$

Note:

Integrals in  $M_{\rho\rho}$ ,  $M_{\rho\phi_n}$ , and  $M_{\phi_n\phi_n}$  include the effect of all parts of the root fitting which flap while integrals in  $M_{\rho e}$ ,  $M_{e\phi_n}$ , and  $M_{e e_1}$  only include the parts of the root fitting which both pitch and flap.

TABLE II.3

## GENERALIZED CENTRIFUGAL FORCE COEFFICIENTS

$$T_{\rho\rho} = I_{z_1}(\text{root}) - I_r$$

$$T_{\rho e_1} = \int_0^R (\lambda + \bar{x}_1 + \phi e_1) r m dr$$

$$T_{\rho \phi_n} = - \int_0^R r f_{\phi_n} m dr = 0$$

$$T_{\rho e_1} = \int_0^R \bar{x}_1 r f_{e_1} m dr$$

$$T_{e_1\rho} = T_{\rho e_1}$$

$$T_{e_1 e_1} = I_{z_1} + \int_0^R \phi^2 m dr - I_{x_1} - \int_0^R (\lambda + e \bar{x}_1) \lambda m dr + \int_0^R \lambda \phi r m dr$$

$$T_{e_1 \phi_n} = \int_0^R f_{\phi_n} (\lambda + \bar{x}_1 + \phi e_1) m dr - \int_0^R e_1 \phi f_{\phi_n}^* m dr + \int_0^R r f_{\phi_n}^* e_1 \lambda m dr$$

$$T_{e_1 e_1} = \int_0^R \left( \frac{dI_{z_1}}{dr} - \frac{dI_{x_1}}{dr} \right) f_{e_1} dr - \int_0^R \bar{x}_1 \lambda f_{e_1} m dr$$

$$T_{\phi_n\rho} = T_{\rho\phi_n}$$

$$T_{\phi_n e_1} = T_{e_1 \phi_n}$$

$$T_{\phi_n \phi_n} = \left( \frac{d f_{\phi_n}}{dr} \right)^2 I_{z_1}(\text{root}) - \int_0^R \left( \frac{d f_{\phi_n}}{dr} \right)^2 \left[ \int_0^R r m dr \right] dr$$

$$T_{\phi_n e_1} = \int_0^R r \bar{x}_1 f_{e_1} \left( \frac{d f_{\phi_n}}{dr} \right) m dr$$

$$T_{e_1\rho} = T_{\rho e_1}$$

$$T_{e_1 e_1} = T_{e_1 e_1}$$

$$T_{e_1 \phi_n} = T_{\phi_n e_1}$$

$$T_{e_1 e_1} = \int_0^R \left( \frac{dI_{z_1}}{dr} \right) f_{e_1}^2 dr - \int_0^R \left( \frac{dI_{x_1}}{dr} \right) f_{e_1}^2 dr - \int_0^R \bar{x}_1 \lambda f_{e_1}^2 m dr$$

TABLE II.4

## GENERALIZED GYROSCOPIC COUPLING COEFFICIENTS

$$2G_{\rho\rho} = 0$$

$$2G_{\rho\phi} = 2I_{z_1} + 2 \int_0^R \phi [\phi + \rho \cdot r] m dr$$

$$2G_{\rho\phi_n} = 2 \int_0^R (\phi + \rho r) f_{\phi_n}^* \phi_0 m dr \quad \dagger$$

$$2G_{\rho\theta} = 2 \int_0^R \left( \frac{dI_z}{dr} \right) f_{\theta} dr$$

$$2G_{\phi\rho} = -2G_{\rho\phi}$$

$$2G_{\theta\rho} = 0$$

$$2G_{\phi\phi_n} = -2 \int_0^R \phi \left[ f_{\phi_n} \rho + \int_0^r \left( \frac{dI_z}{dr} \right) \left( \frac{d\phi}{dr} \right) dr \right] m dr$$

$$2G_{\theta\phi} = 0$$

$$2G_{\phi\rho} = -2G_{\rho\phi}$$

$$2G_{\rho\phi_n} = -2G_{\phi_n\rho}$$

$$2G_{\phi_n\phi_n} = 0$$

$$2G_{\phi\theta} = 0$$

$$2G_{\theta,\rho} = -2G_{\rho\theta}$$

$$2G_{\theta,\phi} = 0$$

$$2G_{\theta,\phi_n} = 0 = -2G_{\phi_n\theta}$$

$$2G_{\theta,\theta} = 0$$

† This term might be neglected. It would be zero if the small bending deflection associated with the flapping mode were included in the analysis.

TABLE II.5

$$A_{\rho\bar{\rho}} = -\pi\rho\int_0^R b^2 r^2 dr$$

$$A_{\rho\bar{\rho}} = -\Omega\rho\int_0^R ab r^2 dr + \rho\Omega\int_0^R (a_{Rr} + a) br^2 dr$$

$$S_{\rho\bar{\rho}} = -\Omega R\rho\int_0^R ab r^2 dr + \rho\Omega R\int_0^R (a_{Rr} + a) br^2 dr$$

$$A_{\rho\rho} = \Omega^2\rho\int_0^R ab(Q + \frac{b}{2})r^2 dr - \rho\Omega^2\int_0^R (a_{Rr} + a)Qr^2 dr + \frac{1}{2}\rho\Omega^2\int_0^R (a_{Rr} - a)b^2 r^2 dr$$

$$C_{\rho\rho} = -\Omega^2 R\rho\int_0^R ab r^2 dr + \rho\Omega^2 R\int_0^R (a_{Rr} + a) br^2 dr$$

$$S_{\rho\rho} = \Omega^2 R\rho\int_0^R ab(Q + \frac{b}{2})rdr + \pi\Omega^2 R\rho\int_0^R b^2 r^2 dr - \rho\Omega^2 R\int_0^R (a_{Rr} + a)bQrdr + \frac{1}{2}\rho\Omega^2 R\int_0^R (a_{Rr} - a)b^2 r^2 dr$$

$$S'_{\rho\rho} = -\frac{1}{2}\Omega^2 R^2\rho\int_0^R ab rdr - \frac{1}{2}\rho\Omega^2 R^2\int_0^R (a_{Rr} + a) brdr$$

$$A_{\rho\bar{\rho}} = \pi\rho\int_0^R b^2 Qrdr$$

$$A_{\rho\bar{\rho}} = \Omega\rho\int_0^R ab(Q + \frac{b}{2})r^2 dr + \pi\Omega\rho\int_0^R b^2 r^2 dr + \rho\Omega\int_0^R (a_{Rr} + a)bQr^2 dr + \rho\Omega\int_0^R (a_{Rr} - a)b^2 r^2 dr$$

$$S_{\rho\bar{\rho}} = \Omega R\rho\int_0^R ab(Q + \frac{b}{2})rdr + \pi\Omega R\rho\int_0^R b^2 r^2 dr - \rho\Omega R\int_0^R (a_{Rr} + a)bQrdr + \frac{1}{2}\rho\Omega R\int_0^R (a_{Rr} - a)b^2 r^2 dr$$

$$A_{\rho\bar{\rho}} = \Omega^2\rho\int_0^R ab r^2 dr - \rho\Omega^2\int_0^R (a_{Rr} + a) br^2 dr - \frac{1}{2}\rho\Omega^2 R^2\int_0^R (a_{Rr} + a) brdr$$

$$S_{\rho\bar{\rho}} = 2\Omega^2 R\rho\int_0^R ab r^2 dr - 2\rho\Omega^2 R\int_0^R (a_{Rr} + a) br^2 dr$$

$$C'_{\rho\bar{\rho}} = -\frac{1}{2}\Omega^2 R^2\rho\int_0^R ab rdr + \frac{1}{2}\rho\Omega^2 R^2\int_0^R (a_{Rr} + a) brdr$$

TABLE II.5 cont'd.

$$A_{ph} = -\pi \rho \int_0^{\infty} b^2 f_h r dr$$

$$A_{ph} = -\Omega \rho \int_0^{\infty} a b f_h r^2 dr + \rho \Omega \int_0^{\infty} (a_{nr} + a) f_h b r^2 dr$$

$$S_{ph} = -\Omega \rho \int_0^{\infty} a b f_h r dr + \rho \Omega R \int_0^{\infty} (a_{nr} + a) f_h b r dr$$

$$A_{ph} = \Omega^2 \rho \int_0^{\infty} a b \left(Q + \frac{b}{2}\right) \frac{df_h}{dr} r^2 dr - \rho \Omega^2 \int_0^{\infty} (a_{nr} + a) Q \frac{df_h}{dr} b r^2 dr + \frac{1}{2} \rho \Omega^2 \int_0^{\infty} (a_{nr} - a) \frac{df_h}{dr} b r^2 dr$$

$$C_{ph} = -\Omega^2 R \rho \int_0^{\infty} a b \frac{df_h}{dr} r^2 dr + \rho \Omega^2 R \int_0^{\infty} (a_{nr} + a) \frac{df_h}{dr} b r^2 dr$$

$$S_{ph} = \Omega^2 R \rho \int_0^{\infty} a b \left(Q + \frac{b}{2}\right) \frac{df_h}{dr} r dr + \pi \Omega^2 R \rho \int_0^{\infty} b^2 \frac{df_h}{dr} r dr - \rho \Omega^2 R \int_0^{\infty} (a_{nr} + a) \frac{df_h}{dr} Q b r dr + \frac{1}{2} \rho \Omega^2 R \int_0^{\infty} (a_{nr} - a) \frac{df_h}{dr} b r dr$$

$$S'_{ph} = -\frac{1}{2} \Omega^2 R^2 \rho \int_0^{\infty} a b \frac{df_h}{dr} r dr + \frac{1}{2} \rho \Omega^2 R^2 \int_0^{\infty} (a_{nr} + a) \frac{df_h}{dr} b r dr$$

$$A_{ph} = \pi \rho \int_0^{\infty} b^2 (Q - \ell) f_h r dr$$

$$A_{ph} = \Omega \rho \int_0^{\infty} a b \left(Q - \ell + \frac{b}{2}\right) f_h r^2 dr + \pi \Omega \rho \int_0^{\infty} b^2 f_h r^2 dr - \rho \Omega \int_0^{\infty} (a_{nr} + a) \chi f_h b r^2 dr + \frac{1}{2} \rho \Omega \int_0^{\infty} (a_{nr} + a) f_h b r^2 dr$$

$$S_{ph} = \Omega R \rho \int_0^{\infty} a b \left(Q - \ell + \frac{b}{2}\right) f_h r dr + \pi \Omega R \rho \int_0^{\infty} b^2 f_h r dr - \rho \Omega R \int_0^{\infty} (a_{nr} + a) \chi f_h b dr + \frac{1}{2} \rho \Omega R \int_0^{\infty} (a_{nr} - a) f_h b r dr$$

$$A_{ph} = \Omega^2 \rho \int_0^{\infty} a b f_h r^2 dr - \rho \Omega^2 \int_0^{\infty} (a_{nr} + a) f_h b r^2 dr - \frac{1}{2} \rho \Omega^2 R^2 \int_0^{\infty} (a_{nr} + a) f_h b r dr$$

$$S_{ph} = 2 \Omega^2 R \rho \int_0^{\infty} a b f_h r^2 dr - 2 \rho \Omega^2 R \int_0^{\infty} (a_{nr} + a) f_h b r^2 dr$$

$$C'_{ph} = -\frac{1}{2} \Omega^2 R^2 \rho \int_0^{\infty} a b f_h r dr + \frac{1}{2} \rho \Omega^2 R^2 \int_0^{\infty} (a_{nr} + a) f_h b r dr$$

TABLE II.5 cont'd.

$$A_{\theta, \ddot{\rho}} = \pi \rho \int_0^{BR} b^2 Q r dr$$

$$A_{\theta, \dot{\rho}} = \Omega \rho \int_0^{BR} ab Q r^2 dr - \pi \Omega \rho \int_0^{BR} b^2 r^2 dr - \rho \Omega \int_0^{BR} (a_{Rr} + a) Q b r^2 dr \\ + \Omega \rho \int_0^{BR} \frac{ab(\theta_0 + \theta_1 - \frac{\omega_0}{\Omega r}) \phi}{r + R \mu \sin \psi} r^3 dr$$

$$S_{\theta, \dot{\rho}} = \Omega R \rho \int_0^{BR} ab Q r dr - \pi \Omega R \rho \int_0^{BR} b^2 r dr - \rho \Omega R \int_0^{BR} (a_{Rr} + a) Q b r dr$$

$$A_{\theta, \rho} = -\Omega^2 \rho \int_0^{BR} ab Q (Q + \frac{b}{2}) r dr + \pi \Omega^2 \rho \int_0^{BR} b^2 Q r dr + \rho \Omega^2 \int_0^{BR} (a_{Rr} + a) Q^2 b r dr - \frac{1}{2} \rho \Omega^2 \int_0^{BR} (a_{Rr} - a) Q b^2 r dr$$

$$C_{\theta, \rho} = \Omega^2 R \rho \int_0^{BR} ab Q r dr - \pi \Omega^2 R \rho \int_0^{BR} b^2 r dr - \rho \Omega^2 R \int_0^{BR} (a_{Rr} + a) Q b r dr \\ + \Omega^2 R \rho \int_0^{BR} \frac{ab(\theta_0 + \theta_1 - \frac{\omega_0}{\Omega r}) \phi}{r + R \mu \sin \psi} r^2 dr$$

$$S_{\theta, \rho} = -\Omega^2 R \rho \int_0^{BR} ab Q (Q + \frac{b}{2}) dr + \rho \Omega^2 R \int_0^{BR} (a_{Rr} + a) Q^2 b dr - \frac{1}{2} \rho \Omega^2 R \int_0^{BR} (a_{Rr} - a) Q b^2 dr$$

$$S'_{\theta, \rho} = \frac{1}{2} \Omega^2 R \rho \int_0^{BR} ab Q dr - \frac{1}{2} \pi \Omega^2 R \rho \int_0^{BR} b^2 dr - \frac{1}{2} \rho \Omega^2 R \int_0^{BR} (a_{Rr} + a) Q b dr$$

$$A_{\theta, \ddot{a}} = -\pi \rho \int_0^{BR} b^2 Q^2 dr$$

$$A_{\theta, \dot{a}} = -\Omega \rho \int_0^{BR} ab Q (Q + \frac{b}{2}) r dr + \rho \Omega \int_0^{BR} (a_{Rr} + a) Q^2 b r dr - \frac{1}{2} \rho \Omega \int_0^{BR} (a_{Rr} - a) Q b^2 r dr$$

$$S_{\theta, \dot{a}} = -\Omega R \rho \int_0^{BR} ab Q (Q + \frac{b}{2}) dr + \rho \Omega R \int_0^{BR} (a_{Rr} + a) Q^2 b dr - \frac{1}{2} \rho \Omega R \int_0^{BR} (a_{Rr} - a) Q b^2 dr$$

$$A_{\theta, a} = -\Omega^2 \rho \int_0^{BR} ab Q r^2 dr + \pi \Omega^2 \rho \int_0^{BR} b^2 r^2 dr + \rho \Omega^2 \int_0^{BR} (a_{Rr} + a) Q b r^2 dr \\ - \Omega^2 \rho \int_0^{BR} ab(\theta_0 + \theta_1 - \frac{\omega_0}{\Omega r}) \phi r^2 dr + \frac{1}{2} \rho \Omega^2 R^2 \mu^2 \int_0^{BR} (a_{Rr} + a) Q r dr$$

TABLE II.5 cont'd.

$$S_{a_0} = -2\Omega^2 R \rho \int_0^{a_0} ab Q r dr + 2\pi \Omega^2 R \rho \int_0^{a_0} b^2 r dr + 2\rho \Omega^2 R \int_0^{a_0} (a_{nr} + a) Q b r dr$$

$$C'_{a_0} = \frac{1}{2} \Omega^2 R^2 \rho \int_0^{a_0} ab Q dr - \frac{1}{2} \pi \Omega^2 R^2 \rho \int_0^{a_0} b^2 dr - \frac{1}{2} \rho \Omega^2 R^2 \int_0^{a_0} (a_{nr} + a) Q b dr$$

$$A_{a_0} = \pi \rho \int_0^{a_0} b^2 f_0 dr$$

$$A_{a_0} = \Omega \rho \int_0^{a_0} ab Q f_0 r dr - \pi \Omega \rho \int_0^{a_0} b^2 f_0 r dr - \rho \Omega \int_0^{a_0} (a_{nr} + a) f_0 Q b r dr \\ + \Omega \rho \int_0^{a_0} \frac{ab(\theta_0 + \theta_1 - \frac{w_0}{Rr})}{r + R\mu \sin \psi} \phi f_0 r^2 dr$$

$$S_{a_0} = \Omega R \rho \int_0^{a_0} ab Q f_0 dr - \pi \Omega R \rho \int_0^{a_0} b^2 f_0 dr - \rho \Omega R \int_0^{a_0} (a_{nr} + a) f_0 Q b dr$$

$$A_{a_0} = -\Omega^2 \rho \int_0^{a_0} ab Q (Q + \frac{b}{2}) \frac{df_0}{dr} r dr + \pi \Omega^2 \rho \int_0^{a_0} b^2 Q \frac{df_0}{dr} r dr + \rho \Omega^2 \int_0^{a_0} (a_{nr} + a) \frac{df_0}{dr} Q b r dr \\ - \Omega^2 \rho \int_0^{a_0} ab (\theta_0 - \theta_1 - \frac{w_0}{Rr}) (\theta_0 - \frac{w_0}{Rr}) f_0^* r^2 dr + \Omega^2 \rho \int_0^{a_0} C_{a_0} b f_0^* r^2 dr - \rho \Omega^2 \int_0^{a_0} (a_{nr} - a) \frac{df_0}{dr} Q b r dr$$

$$C_{a_0} = \Omega^2 R \rho \int_0^{a_0} ab Q \frac{df_0}{dr} r dr - \pi \Omega^2 R \rho \int_0^{a_0} b^2 \frac{df_0}{dr} r dr - \rho \Omega^2 R \int_0^{a_0} (a_{nr} + a) \frac{df_0}{dr} Q b r dr \\ + \Omega^2 R \rho \int_0^{a_0} ab \frac{(\theta_0 + \theta_1 - \frac{w_0}{Rr})}{r + R\mu \sin \psi} \phi \frac{df_0}{dr} r^2 dr$$

$$S_{a_0} = -\Omega^2 R \rho \int_0^{a_0} ab Q (Q + \frac{b}{2}) \frac{df_0}{dr} dr - \pi \Omega^2 R \rho \int_0^{a_0} b^2 Q \frac{df_0}{dr} dr + \rho \Omega R \int_0^{a_0} (a_{nr} + a) \frac{df_0}{dr} Q b dr - \frac{1}{2} \rho \Omega R \int_0^{a_0} (a_{nr} - a) \frac{df_0}{dr} Q b dr$$

$$S'_{a_0} = \frac{1}{2} \Omega^2 R \rho \int_0^{a_0} ab Q \frac{df_0}{dr} dr - \frac{1}{2} \pi \Omega^2 R \rho \int_0^{a_0} b^2 \frac{df_0}{dr} dr - \frac{1}{2} \rho \Omega^2 R \int_0^{a_0} (a_{nr} + a) \frac{df_0}{dr} Q b dr$$

TABLE II.5 cont'd.

$$A_{a\beta} = -\pi\rho\int_0^{2\pi} b^2 Q(Q-l)f_\beta dr$$

$$A_{a\beta} = -\Omega\rho\int_0^{2\pi} abQ(Q-l+\frac{b}{2})f_\beta r dr - \pi\Omega\rho\int_0^{2\pi} b^2 l f_\beta r dr + \rho\Omega\int_0^{2\pi} (a_{nr}+a)x_\beta f_\alpha Q b r dr - \frac{1}{2}\rho\Omega\int_0^{2\pi} (a_{nr}-a)f_\alpha Q b^2 r dr$$

$$S_{a\beta} = -\Omega R\rho\int_0^{2\pi} abQ(Q-l+\frac{b}{2})f_\beta dr - \pi\Omega R\rho\int_0^{2\pi} b^2 l f_\beta dr + \rho\Omega R\int_0^{2\pi} (a_{nr}+a)x_\beta f_\alpha Q b dr - \frac{1}{2}\rho\Omega R\int_0^{2\pi} (a_{nr}-a)f_\alpha Q b^2 dr$$

$$A_{a\alpha} = -\Omega^2\rho\int_0^{2\pi} abQ f_\alpha r^2 dr + \pi\Omega^2\rho\int_0^{2\pi} b^2 l f_\alpha r^2 dr + \rho\Omega^2\int_0^{2\pi} (a_{nr}+a)f_\alpha Q b r^2 dr$$

$$S_{a\alpha} = -2\Omega^2 R\rho\int_0^{2\pi} abQ f_\alpha r dr + 2\pi\Omega^2 R\rho\int_0^{2\pi} b^2 l f_\alpha r dr + 2\rho\Omega^2 R\int_0^{2\pi} (a_{nr}+a)f_\alpha Q b r dr$$

$$C'_{a\alpha} = \frac{1}{2}\Omega^2 R^2\rho\int_0^{2\pi} abQ f_\alpha dr - \frac{1}{2}\pi\Omega^2 R^2\rho\int_0^{2\pi} b^2 l f_\alpha dr - \frac{1}{2}\rho\Omega^2 R^2\int_0^{2\pi} (a_{nr}+a)f_\alpha Q b dr$$

$$A_{\phi\beta} = -\pi\rho\int_0^{2\pi} b^2 f_\beta r dr$$

$$A_{\phi\beta} = -\Omega\rho\int_0^{2\pi} ab f_\beta r^2 dr + \rho\Omega\int_0^{2\pi} (a_{nr}+a)f_\beta b r^2 dr$$

$$S_{\phi\beta} = -\Omega R\rho\int_0^{2\pi} ab f_\beta r dr + \rho\Omega R\int_0^{2\pi} (a_{nr}+a)f_\beta b r dr$$

$$A_{\phi\alpha} = \Omega^2\rho\int_0^{2\pi} ab(Q+\frac{b}{2})f_\alpha r dr - \rho\Omega^2\int_0^{2\pi} (a_{nr}+a)f_\alpha Q b r dr + \frac{1}{2}\rho\Omega^2\int_0^{2\pi} (a_{nr}-a)f_\alpha b^2 r dr$$

$$C_{\phi\alpha} = -\Omega^2 R\rho\int_0^{2\pi} ab f_\alpha r dr - \rho\Omega^2 R\int_0^{2\pi} (a_{nr}+a)f_\alpha b r dr$$

$$S_{\phi\alpha} = \Omega^2 R\rho\int_0^{2\pi} ab(Q+\frac{b}{2})f_\alpha dr + \pi\Omega^2 R\rho\int_0^{2\pi} b^2 l f_\alpha dr - \rho\Omega^2 R\int_0^{2\pi} (a_{nr}+a)f_\alpha Q b dr + \frac{1}{2}\rho\Omega^2 R\int_0^{2\pi} (a_{nr}-a)f_\alpha b^2 dr$$

$$S'_{\phi\alpha} = -\frac{1}{2}\Omega^2 R^2\rho\int_0^{2\pi} ab f_\alpha dr + \frac{1}{2}\rho\Omega^2 R^2\int_0^{2\pi} (a_{nr}+a)f_\alpha b dr$$

TABLE II.5 cont'd.

$$\begin{aligned}
A_{42} &= \pi \rho \int_0^{\infty} b^2 Q f_4 r dr \\
A_{44} &= \Omega \rho \int_0^{\infty} ab(Q + \frac{b}{2}) f_4 r dr + \pi \Omega \rho \int_0^{\infty} b^2 f_4 r dr - \rho \Omega \int_0^{\infty} (a_{\infty} + a) f_4 Q b r dr - \rho \Omega \int_0^{\infty} (a_{\infty} - a) f_4 b r dr \\
S_{42} &= \Omega R \rho \int_0^{\infty} ab(Q + \frac{b}{2}) f_4 r dr + \pi \Omega R \rho \int_0^{\infty} b^2 f_4 r dr - \rho \Omega R \int_0^{\infty} (a_{\infty} + a) f_4 Q b r dr + \rho \Omega R \int_0^{\infty} (a_{\infty} - a) f_4 b r dr \\
A_{44} &= \Omega \rho \int_0^{\infty} ab f_4 r dr - \rho \Omega \int_0^{\infty} (a_{\infty} + a) f_4 b r dr - \frac{1}{2} \rho \Omega R \int_0^{\infty} f_4 (a_{\infty} + a) f_4 b r dr \\
S_{44} &= 2 \Omega^2 R \rho \int_0^{\infty} ab f_4 r dr - 2 \rho \Omega R \int_0^{\infty} (a_{\infty} + a) f_4 b r dr \\
C_{44} &= -\frac{1}{2} \Omega^2 R \rho \int_0^{\infty} ab f_4 r dr + \frac{1}{2} \rho \Omega R \int_0^{\infty} (a_{\infty} + a) f_4 b r dr \\
A_{44} &= -\pi \rho \int_0^{\infty} b^2 f_4 r dr \\
A_{44} &= -\Omega \rho \int_0^{\infty} ab f_4 r dr + \rho \Omega \int_0^{\infty} (a_{\infty} + a) f_4 b r dr \\
S_{44} &= -\Omega R \rho \int_0^{\infty} ab f_4 r dr + \rho \Omega R \int_0^{\infty} (a_{\infty} + a) f_4 b r dr \\
A_{44} &= \Omega \rho \int_0^{\infty} ab(Q + \frac{b}{2}) \frac{df_4}{dr} f_4 r dr - \rho \Omega \int_0^{\infty} (a_{\infty} + a) \frac{df_4}{dr} f_4 Q b r dr + \rho \Omega \int_0^{\infty} (a_{\infty} - a) \frac{df_4}{dr} f_4 b r dr \\
C_{44} &= -\Omega^2 R \rho \int_0^{\infty} ab \frac{df_4}{dr} f_4 r dr + \rho \Omega R \int_0^{\infty} (a_{\infty} + a) \frac{df_4}{dr} f_4 b r dr \\
S_{44} &= \Omega^2 R \rho \int_0^{\infty} ab(Q + \frac{b}{2}) \frac{df_4}{dr} f_4 r dr + \pi \Omega^2 R \rho \int_0^{\infty} b^2 \frac{df_4}{dr} f_4 r dr - \rho \Omega R \int_0^{\infty} (a_{\infty} + a) \frac{df_4}{dr} f_4 Q b r dr + \frac{1}{2} \rho \Omega R \int_0^{\infty} (a_{\infty} - a) \frac{df_4}{dr} f_4 b r dr \\
S_{44} &= -\frac{1}{2} \Omega^2 R \rho \int_0^{\infty} ab \frac{df_4}{dr} f_4 r dr + \rho \Omega R \int_0^{\infty} (a_{\infty} + a) \frac{df_4}{dr} f_4 b r dr
\end{aligned}$$

TABLE II.5 cont'd.

$$\begin{aligned}
A_{43} &= \pi \rho \int_0^{\infty} b^2 (Q-L) f_0^2 f_0' dr \\
A_{43} &= \Omega \rho \int_0^{\infty} ab (Q-L + \frac{b}{2}) f_0^2 f_0' r dr + \pi \Omega \rho \int_0^{\infty} b^2 f_0^2 f_0' r dr \\
S_{43} &= \Omega R \rho \int_0^{\infty} ab (Q-L + \frac{b}{2}) f_0^2 f_0' dr + \pi \Omega R \rho \int_0^{\infty} b^2 f_0^2 f_0' dr \\
A_{44} &= \Omega \rho \int_0^{\infty} ab f_0^2 f_0' r dr - \rho \Omega \int_0^{\infty} (a_m + a) f_0^2 f_0' b r^2 dr \\
S_{44} &= 2 \Omega^2 R \rho \int_0^{\infty} ab f_0^2 f_0' r dr - 2 \rho \Omega R \int_0^{\infty} (a_m + a) f_0^2 f_0' b r dr \\
C'_{44} &= -\frac{1}{2} \Omega^2 R^2 \rho \int_0^{\infty} ab f_0^2 f_0' dr - \rho \Omega^2 R^2 \int_0^{\infty} (a_m + a) f_0^2 f_0' b dr \\
^{32} A_{44} &= \pi \rho \int_0^{\infty} b^2 (Q-L) f_0^2 f_0' dr \\
A_{44} &= \Omega \rho \int_0^{\infty} ab (Q-L) f_0^2 f_0' r dr - \pi \Omega \rho \int_0^{\infty} b^2 f_0^2 f_0' r^2 dr - \rho \Omega \int_0^{\infty} (a_m + a) b (Q-L) f_0^2 f_0' r^2 dr \\
S_{44} &= \Omega R \rho \int_0^{\infty} ab (Q-L) f_0^2 f_0' r dr - \pi \Omega R \rho \int_0^{\infty} b^2 f_0^2 f_0' r dr - \rho \Omega^2 R \int_0^{\infty} (a_m + a) b (Q-L) f_0^2 f_0' r dr \\
A_{44} &= -\Omega^2 \rho \int_0^{\infty} ab (Q-L) (Q + \frac{b}{2}) f_0^2 f_0' r dr + \pi \Omega^2 \rho \int_0^{\infty} b^2 Q f_0^2 f_0' r dr + \rho \Omega^2 \int_0^{\infty} (a_m + a) b (Q-L) Q f_0^2 f_0' r dr - \frac{1}{2} \rho \Omega^2 \int_0^{\infty} (a_m - a) f_0^2 f_0' (Q-L) f_0' r dr \\
C_{44} &= \Omega^2 R \rho \int_0^{\infty} ab (Q-L) f_0^2 f_0' r dr - \pi \Omega^2 R \rho \int_0^{\infty} b^2 f_0^2 f_0' r dr - \rho \Omega^2 R \int_0^{\infty} (a_m + a) b (Q-L) f_0^2 f_0' r dr \\
S_{44} &= -\Omega^2 R \rho \int_0^{\infty} ab (Q-L) (Q + \frac{b}{2}) f_0^2 f_0' r dr + \pi \Omega^2 R \rho \int_0^{\infty} b^2 L f_0^2 f_0' r dr + \rho \Omega^2 R \int_0^{\infty} (a_m + a) b (Q-L) Q f_0^2 f_0' r dr - \frac{1}{2} \rho \Omega^2 R \int_0^{\infty} (a_m - a) f_0^2 f_0' (Q-L) f_0' r dr \\
S'_{44} &= \frac{1}{2} \Omega^2 R^2 \rho \int_0^{\infty} ab (Q-L) f_0^2 f_0' dr - \frac{1}{2} \pi \Omega^2 R^2 \rho \int_0^{\infty} b^2 f_0^2 f_0' dr - \frac{1}{2} \rho \Omega^2 R^2 \int_0^{\infty} (a_m + a) b (Q-L) f_0^2 f_0' dr
\end{aligned}$$

$$\begin{aligned}
A_{q,q} &= -\pi \rho \int_0^{\infty} b^2 Q(Q-1) f_q dr \\
A_{q,q} &= -\Omega \rho \int_0^{\infty} ab(Q-1)(Q+\frac{b}{2}) f_q dr + \pi \Omega \rho \int_0^{\infty} b^2 l f_q dr + \rho \Omega \int_0^{\infty} (a_{nr}+a)b(Q-1)Q f_q dr - \frac{1}{2} \rho \Omega \int_0^{\infty} (a_{nr}-a)b^2(Q-1) f_q dr \\
S_{q,q} &= -\Omega R \rho \int_0^{\infty} ab(Q-1)(Q+\frac{b}{2}) f_q dr + \pi \Omega R \rho \int_0^{\infty} b^2 l f_q dr - \rho \Omega R \int_0^{\infty} (a_{nr}+a)b(Q-1)Q f_q dr - \frac{1}{2} \rho \Omega R \int_0^{\infty} (a_{nr}-a)b^2(Q-1) f_q dr \\
A_{q,q} &= -\Omega^2 \rho \int_0^{\infty} ab(Q-1) f_q r^2 dr + \pi \Omega^2 \rho \int_0^{\infty} b^2 l f_q r^2 dr + \rho \Omega^2 \int_0^{\infty} (a_{nr}+a)b(Q-1) f_q r^2 dr \\
S_{q,q} &= -2 \Omega^2 R \rho \int_0^{\infty} ab(Q-1) f_q r dr + 2 \pi \Omega^2 R \rho \int_0^{\infty} b^2 l f_q r dr + 2 \rho \Omega^2 R \int_0^{\infty} (a_{nr}+a)b(Q-1) f_q r dr \\
C'_{q,q} &= \frac{1}{2} \Omega^2 R^2 \rho \int_0^{\infty} ab(Q-1) f_q dr - \frac{1}{2} \pi \Omega^2 R^2 \rho \int_0^{\infty} b^2 l f_q dr - \frac{1}{2} \rho \Omega^2 R^2 \int_0^{\infty} (a_{nr}+a)b(Q-1) f_q dr \\
A_{q,l} &= \pi \rho \int_0^{\infty} b^2(Q-1) f_q f_l dr \\
A_{q,l} &= \Omega \rho \int_0^{\infty} ab(Q-1) f_q f_l dr - \pi \Omega \rho \int_0^{\infty} b^2 l f_q f_l dr - \rho \Omega \int_0^{\infty} (a_{nr}+a)b(Q-1) f_q f_l dr \\
S_{q,l} &= \Omega R \rho \int_0^{\infty} ab(Q-1) f_q f_l dr - \pi \Omega R \rho \int_0^{\infty} b^2 l f_q f_l dr - \rho \Omega R \int_0^{\infty} (a_{nr}+a)b(Q-1) f_q f_l dr \\
A_{q,l} &= -\Omega^2 \rho \int_0^{\infty} ab(Q-1)(Q+\frac{b}{2}) \frac{df_q}{dr} f_l dr + \pi \Omega^2 \rho \int_0^{\infty} b^2 Q \frac{df_q}{dr} f_l dr + \rho \Omega^2 \int_0^{\infty} (a_{nr}+a)b(Q-1)Q f_q \frac{df_l}{dr} dr - \frac{1}{2} \rho \Omega^2 \int_0^{\infty} (a_{nr}-a)b^2(Q-1) f_q \frac{df_l}{dr} dr \\
C_{q,l} &= \Omega R \rho \int_0^{\infty} ab(Q-1) \frac{df_q}{dr} f_l dr - \pi \Omega^2 R \rho \int_0^{\infty} b^2 \frac{df_q}{dr} f_l dr - \rho \Omega^2 R \int_0^{\infty} (a_{nr}+a)b(Q-1) f_q \frac{df_l}{dr} dr \\
S_{q,l} &= -\Omega^2 R \rho \int_0^{\infty} ab(Q-1)(Q+\frac{b}{2}) \frac{df_q}{dr} f_l dr + \pi \Omega^2 R \rho \int_0^{\infty} b^2 Q \frac{df_q}{dr} f_l dr + \rho \Omega^2 R \int_0^{\infty} (a_{nr}+a)b(Q-1)Q f_q \frac{df_l}{dr} dr - \frac{1}{2} \rho \Omega^2 R \int_0^{\infty} (a_{nr}-a)b^2(Q-1) f_q \frac{df_l}{dr} dr \\
S'_{q,l} &= \frac{1}{2} \Omega^2 R^2 \rho \int_0^{\infty} ab(Q-1) \frac{df_q}{dr} f_l dr - \frac{1}{2} \pi \Omega^2 R^2 \rho \int_0^{\infty} b^2 \frac{df_q}{dr} f_l dr - \rho \Omega^2 R^2 \int_0^{\infty} (a_{nr}+a)b(Q-1) f_q \frac{df_l}{dr} dr
\end{aligned}$$

TABLE II.5 cont'd.

$$\begin{aligned}
A_{\theta\theta} &= -\pi\rho\int_0^{2\pi} b^2(Q-l)f_a^2 dr \\
A_{\theta\dot{\theta}} &= -\Omega\rho\int_0^{2\pi} ab(Q-l)(Q-l+\frac{b}{2})f_a^2 r dr + \rho\Omega\int_0^{2\pi} (a_{ne}+a)b(Q-l)\chi_1 f_a^2 r dr - \frac{1}{2}\rho\Omega\int_0^{2\pi} (a_{ne}-a)b^2(Q-l)f_a^2 r dr \\
S_{\theta\dot{\theta}} &= -\Omega R\rho\int_0^{2\pi} ab(Q-l)(Q-l+\frac{b}{2})f_a^2 dr + \rho\Omega R\int_0^{2\pi} (a_{ne}+a)b(Q-l)\chi_1 f_a^2 dr - \frac{1}{2}\rho\Omega R\int_0^{2\pi} (a_{ne}-a)b^2(Q-l)f_a^2 dr \\
A_{\theta\ddot{\theta}} &= -\Omega^2\rho\int_0^{2\pi} ab(Q-l)f_a^2 r^2 dr + \pi\Omega^2\rho\int_0^{2\pi} b^2 f_a^2 r^2 dr + \rho\Omega^2\int_0^{2\pi} (a_{ne}+a)b(Q-l)f_a^2 r^2 dr \\
S_{\theta\ddot{\theta}} &= -2\Omega^2 R\rho\int_0^{2\pi} ab(Q-l)f_a^2 r dr + 2\pi\Omega^2 R\rho\int_0^{2\pi} b^2 f_a^2 r dr + 2\rho\Omega^2 R\int_0^{2\pi} (a_{ne}+a)b(Q-l)f_a^2 r dr \\
C'_{\theta\ddot{\theta}} &= \frac{1}{2}\Omega^2 R^2\rho\int_0^{2\pi} ab(Q-l)f_a^2 dr - \frac{1}{2}\pi\Omega^2 R^2\rho\int_0^{2\pi} b^2 f_a^2 dr - \frac{1}{2}\rho\Omega^2 R^2\int_0^{2\pi} (a_{ne}+a)b(Q-l)f_a^2 dr
\end{aligned}$$



Figure 1a HELICOPTER FLUTTER MODEL INSTALLATION ON SMALL ROTORCRAFT TEST APPARATUS-SIDE VIEW

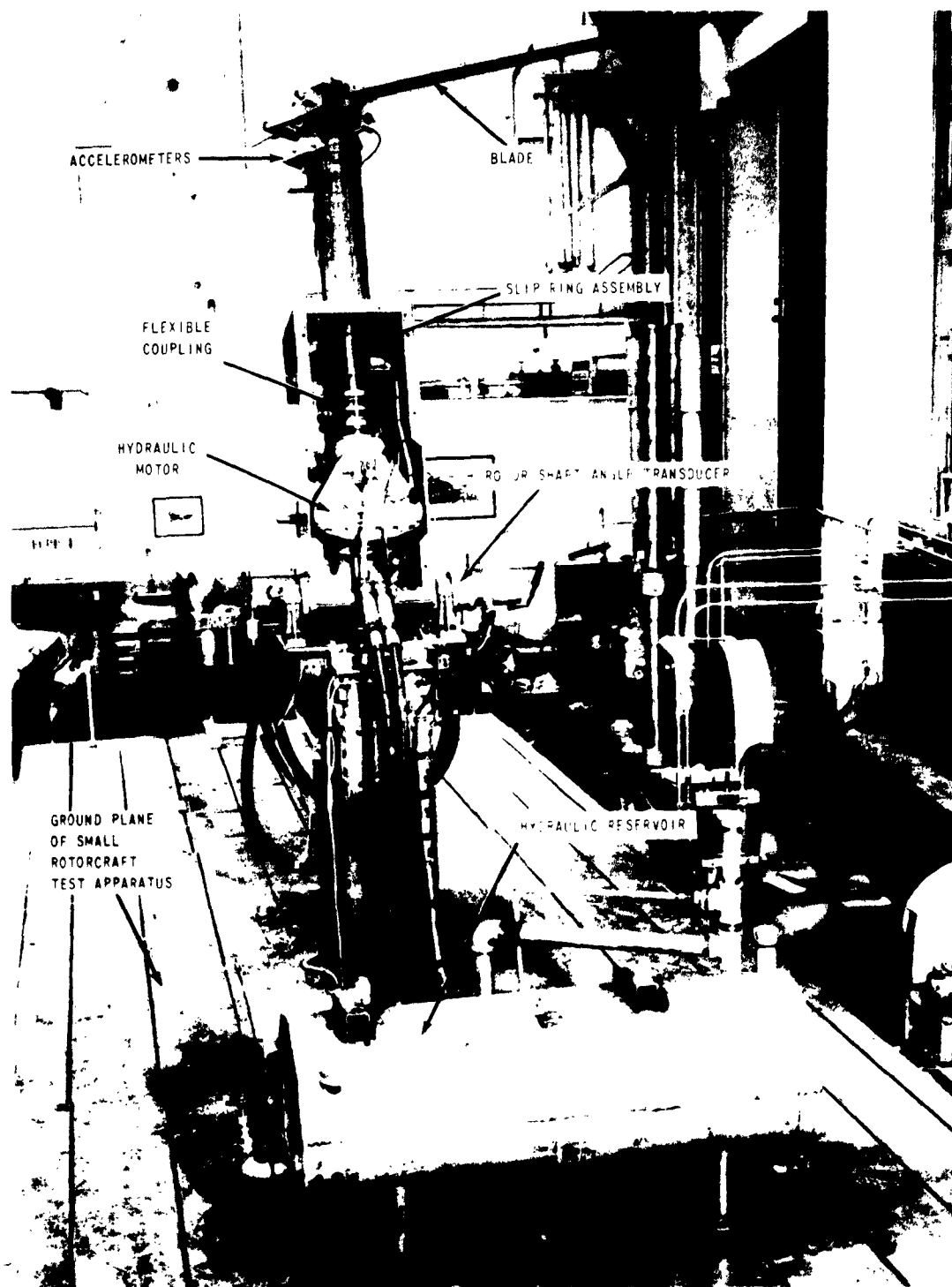


Figure 1b HELICOPTER FLUTTER MODEL INSTALLATION ON SMALL ROTORCRAFT TEST TRAILER—VIEW LOOKING FORWARD

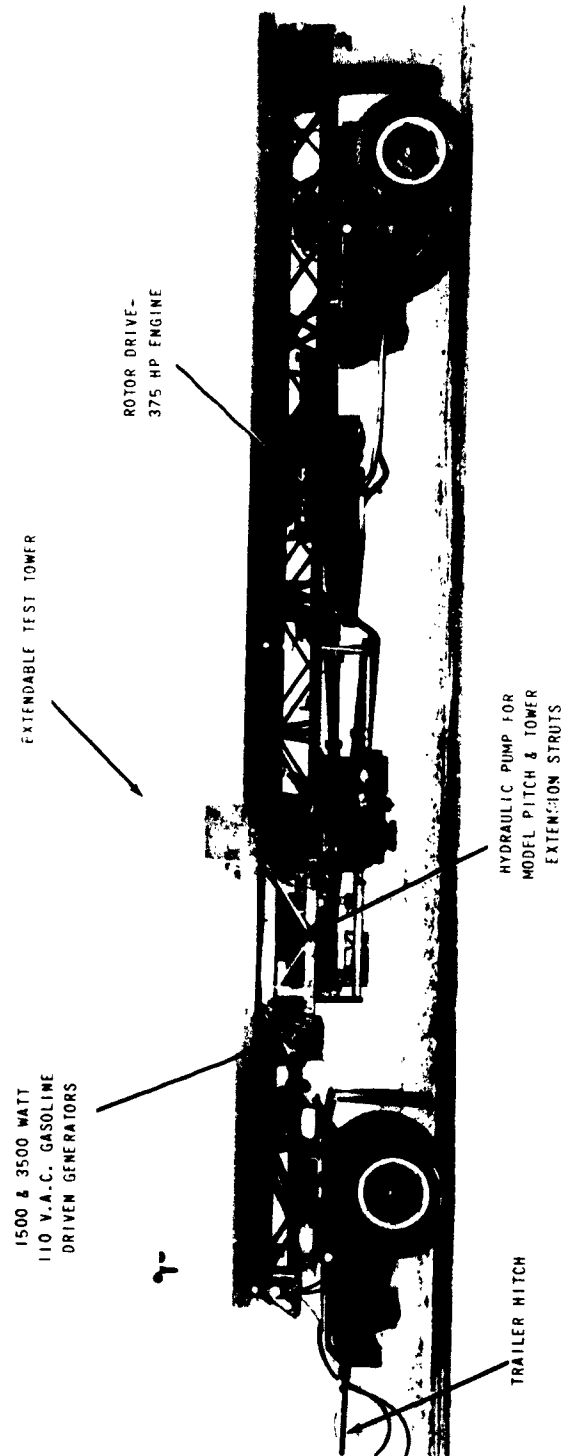


Figure 2 SMALL ROTORCRAFT TEST TRAILER

TEST OPERATORS  
POSITION

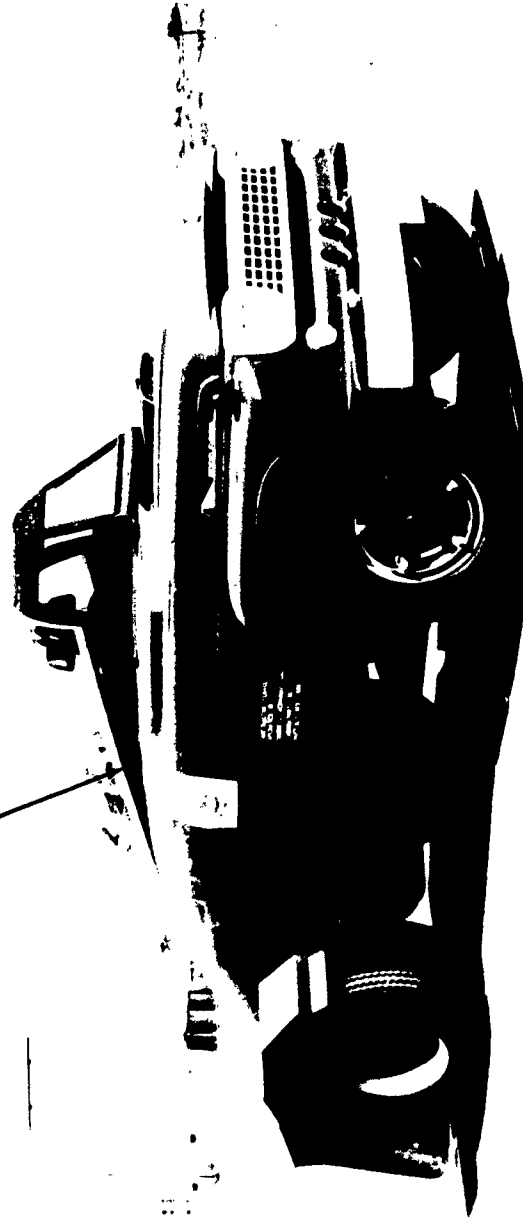


Figure 3 TRACTOR FOR SMALL ROTORCRAFT TEST APPARATUS

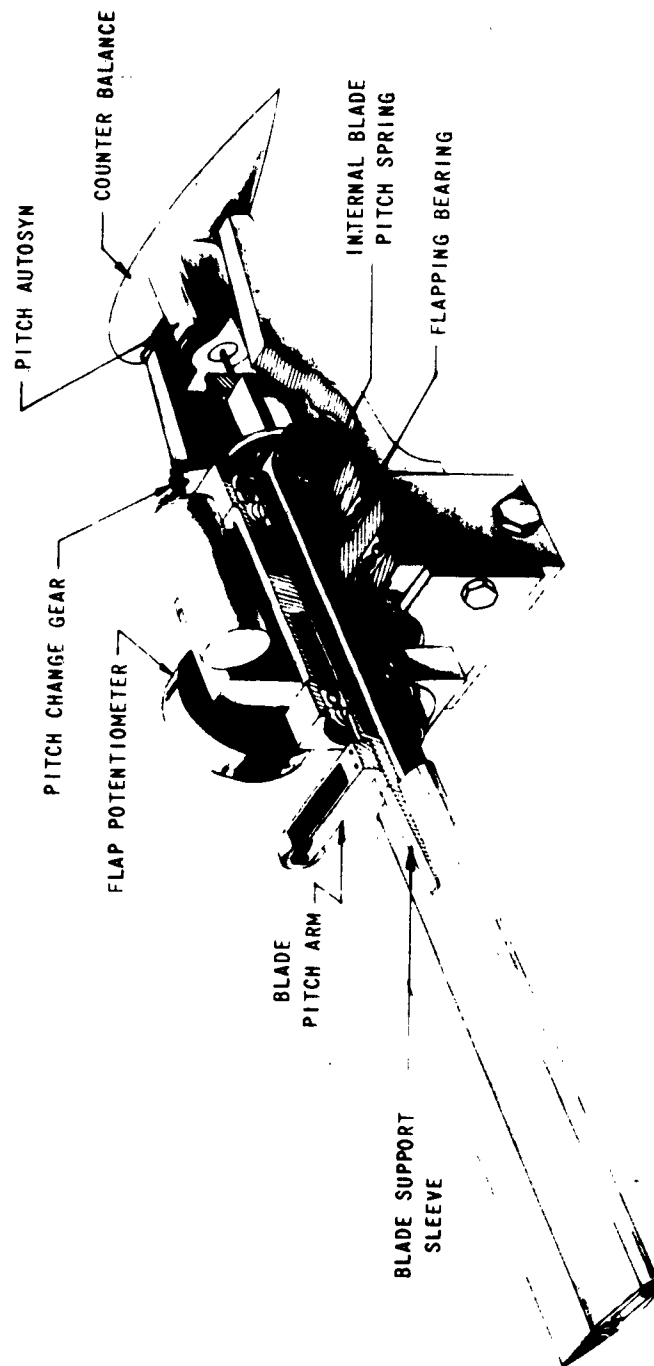


Figure 4 HEAD - HELICOPTER FLUTTER MODEL

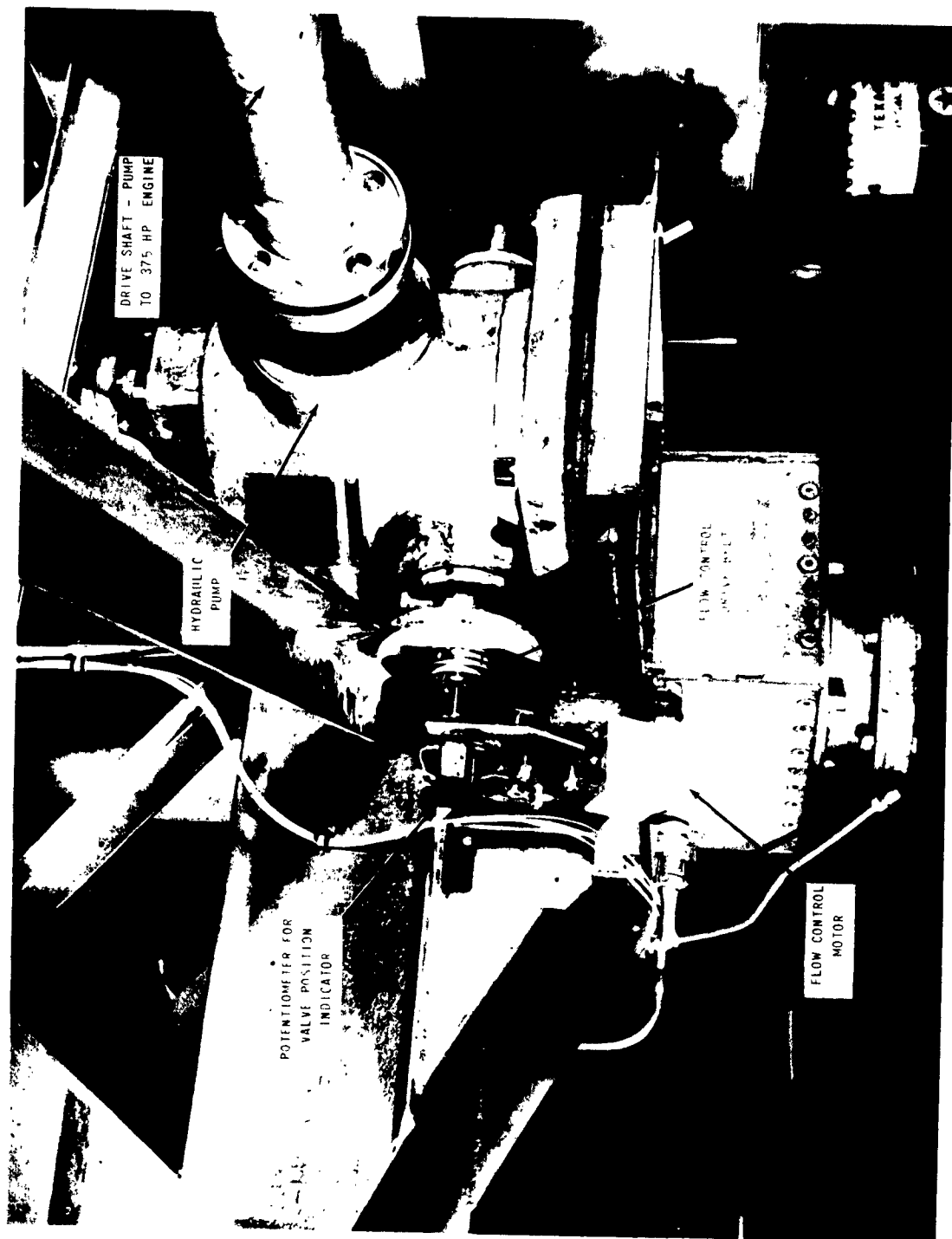


Figure 5 ROTOR HYDRAULIC PUMP

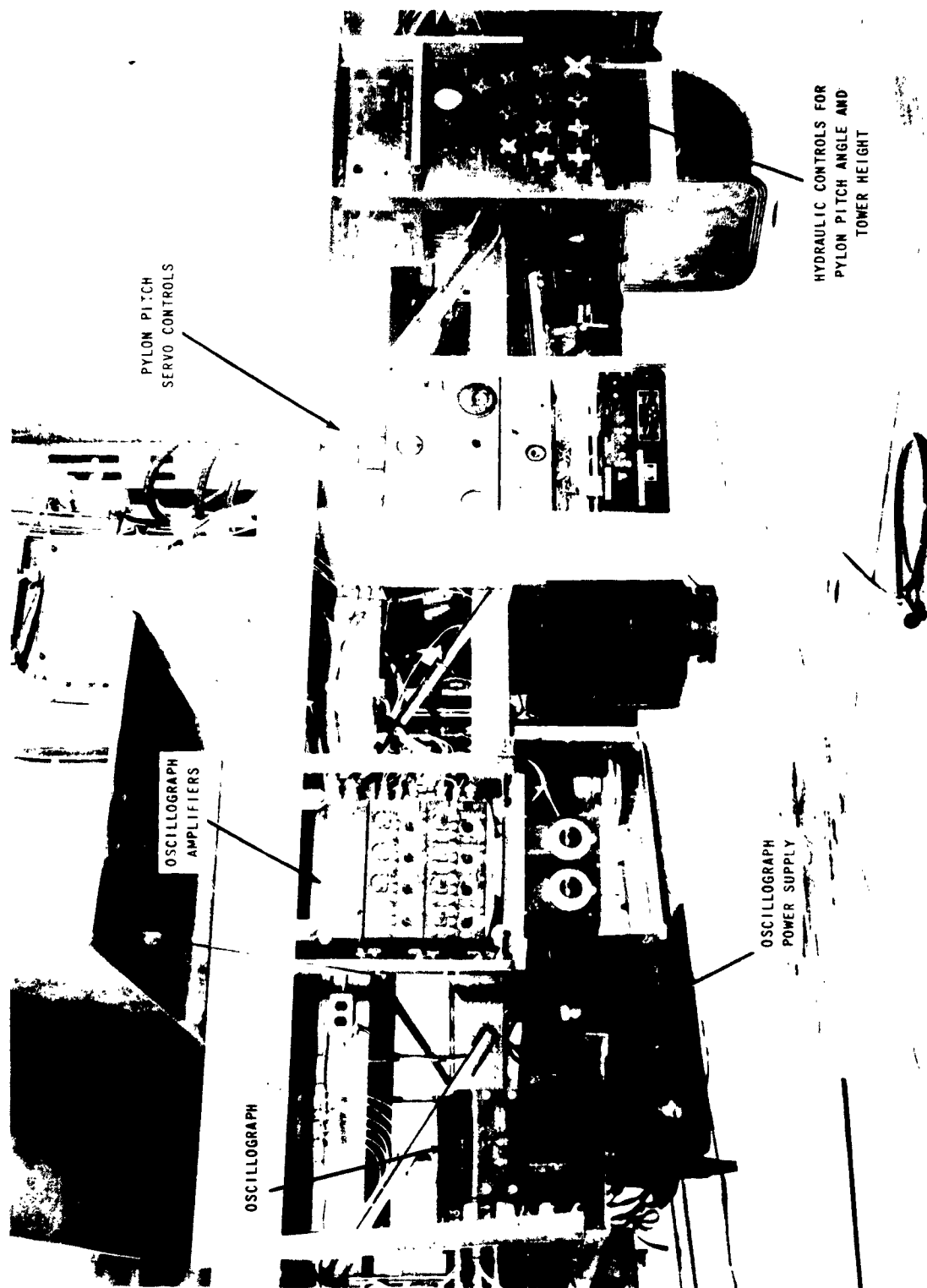


Figure 6 INSTRUMENTATION AND CONTROL PANELS - SMALL ROTORCRAFT TEST TRAILER

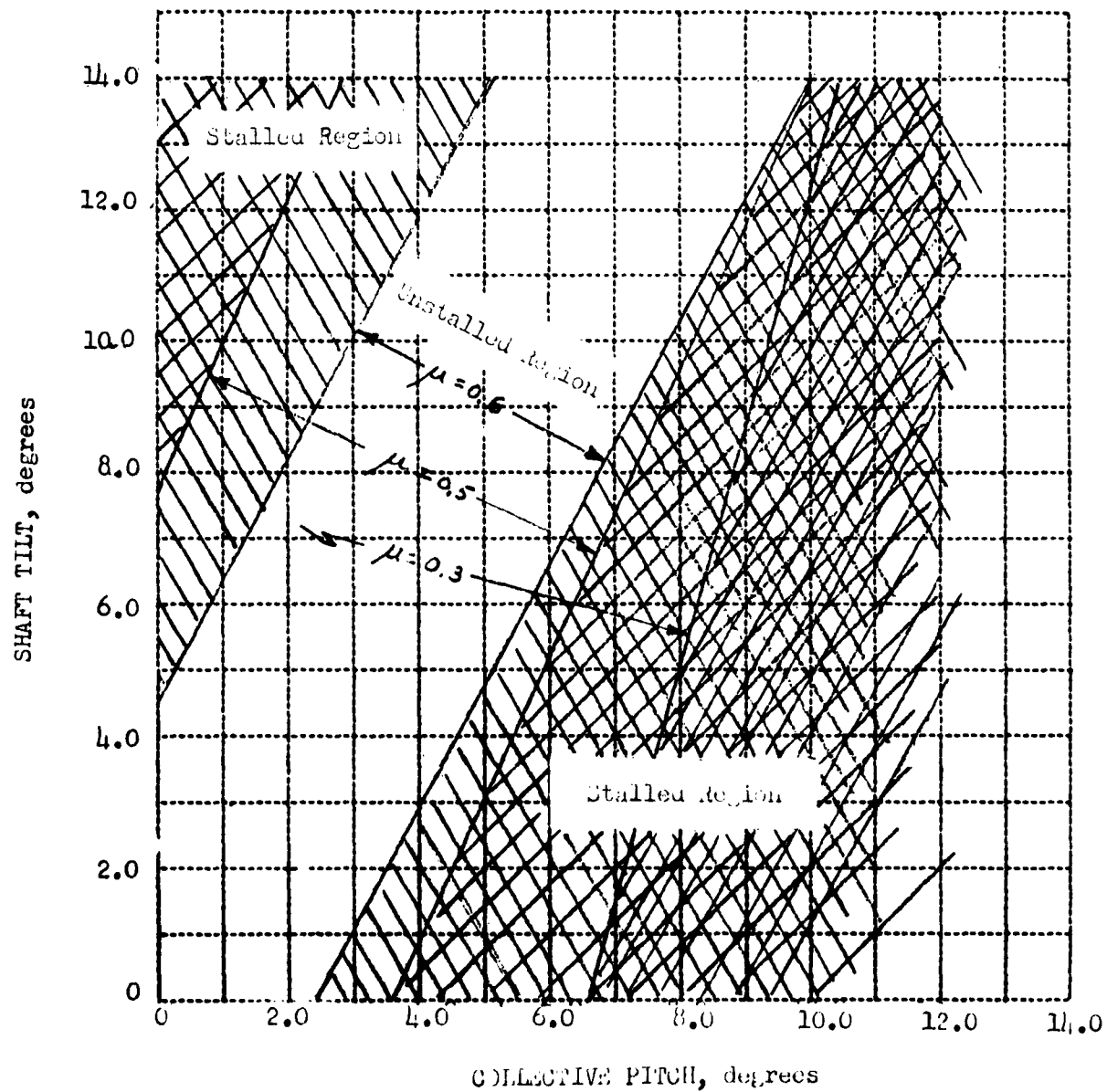


Figure 7 Approximate Stall Regions for Retreating Blade Tip of the Model Rotor as Functions of Collective Pitch and Rotor Shaft Tilt

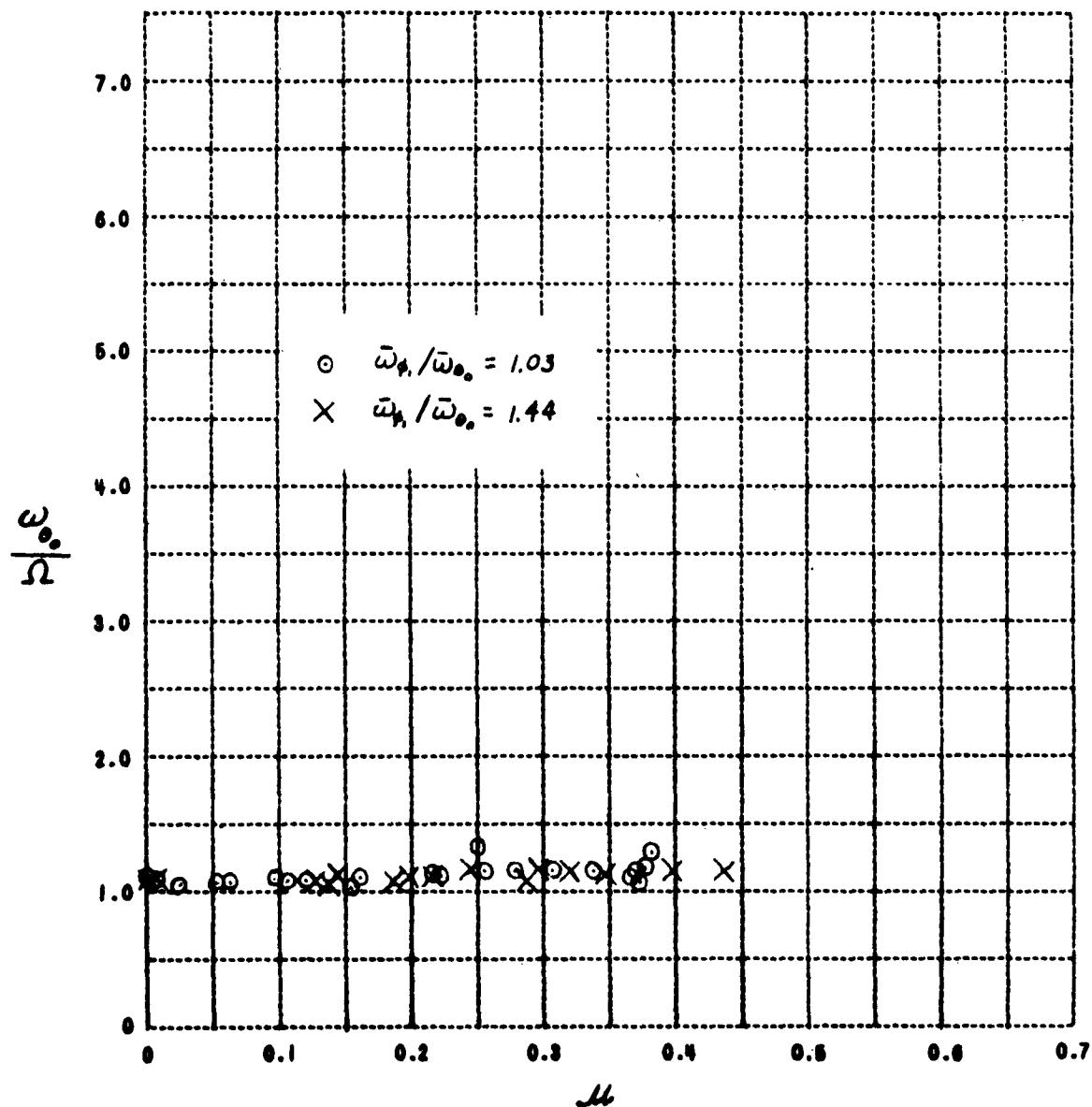


Figure 8a EXPERIMENTAL FLUTTER DATA : [NONROTATING PITCHING  
FREQUENCY / SHAFT ROTATIONAL SPEED] vs ADVANCE RATIO

$$\bar{x}_e / c = 0.0036, \quad \bar{\omega}_f / \bar{\omega}_{0.0} = 1.03 \text{ and } 1.44;$$

$$3^\circ < \theta_0 < 4^\circ$$

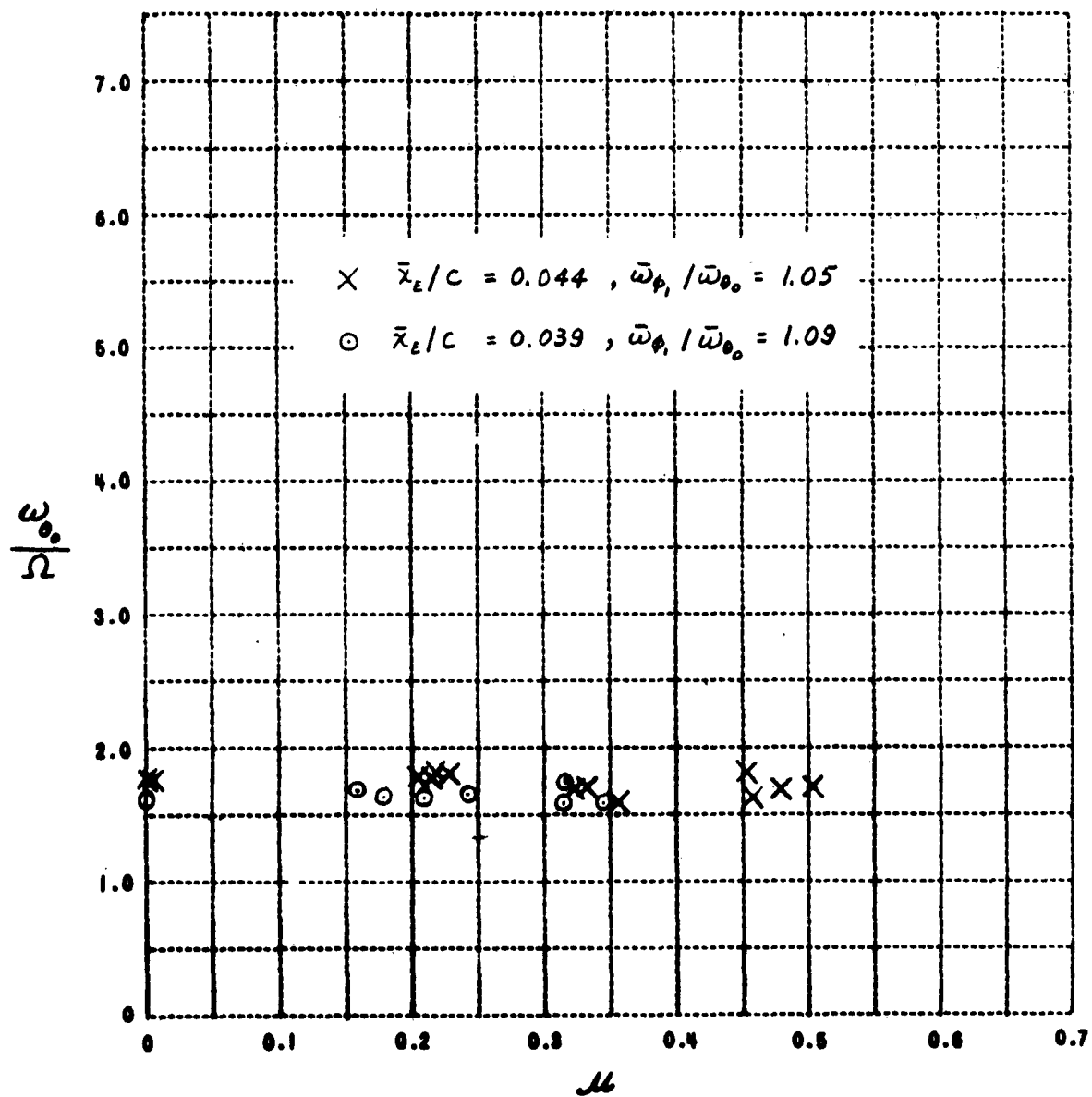


Figure 8b  $\bar{x}_e/c = 0.044, \bar{\omega}_\phi/\bar{\omega}_0 = 1.05$  and  
 $\bar{x}_e/c = 0.039, \bar{\omega}_\phi/\bar{\omega}_0 = 1.09;$   
 $3.5^\circ < \theta_0 < 5.5^\circ$

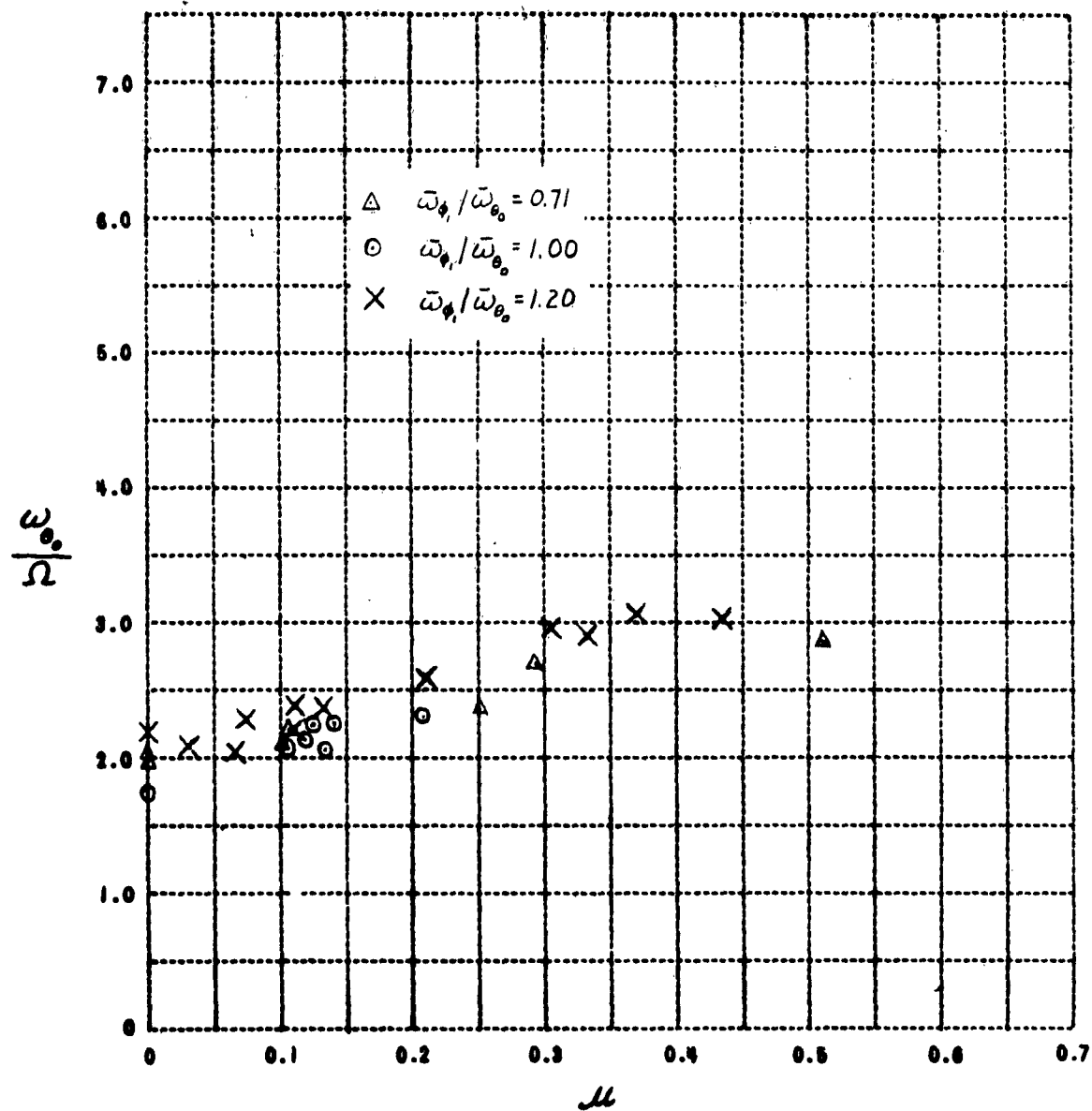


Figure 8c  $\bar{x}_r/C = 0.057$ ,  $\bar{\omega}_\theta/\bar{\omega}_{\theta_0} = 0.71, 1.00, \text{ and } 1.20$ ;  
 $2^\circ < \theta_0 < 6^\circ$

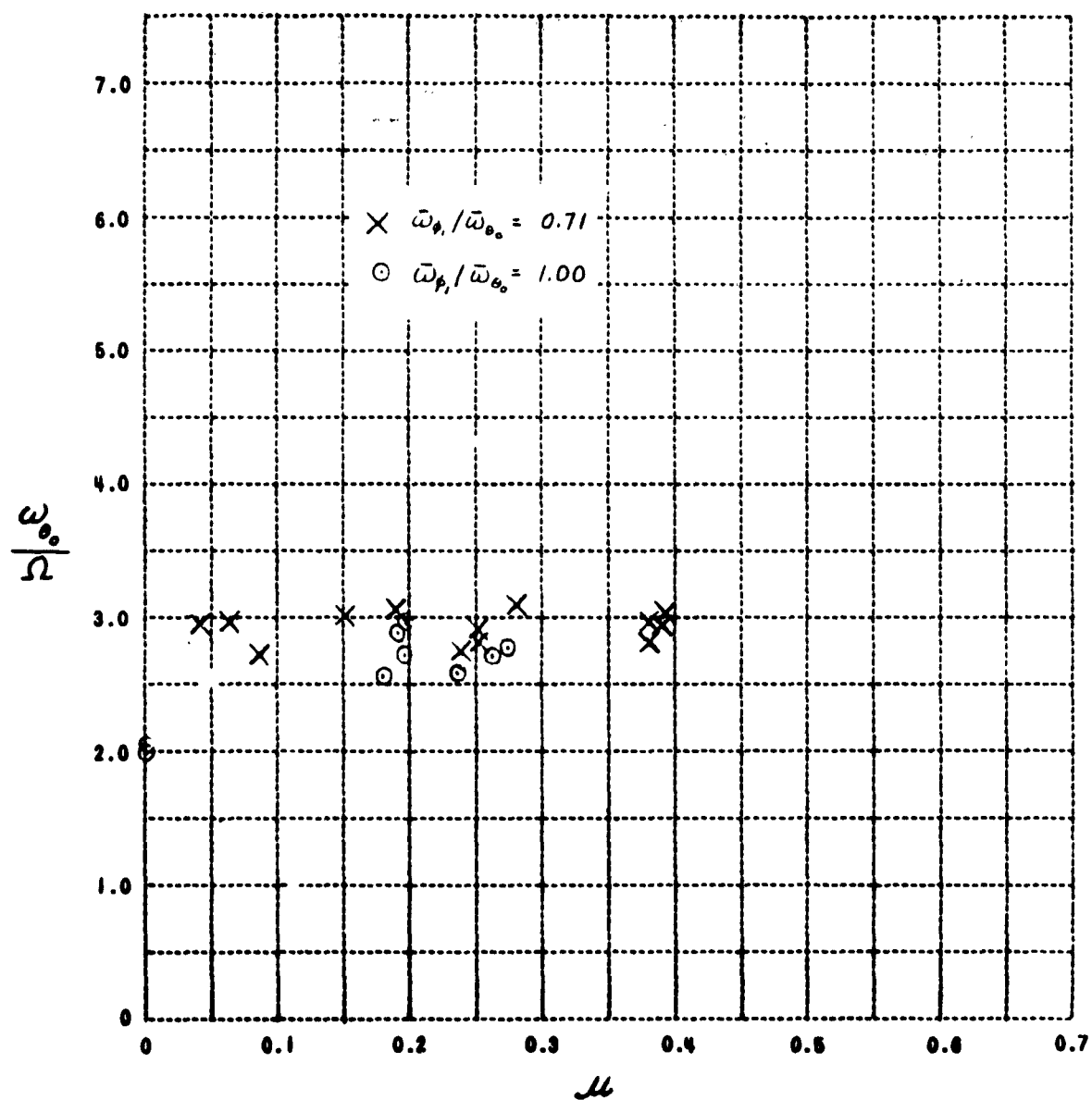


Figure 8d  $\bar{\lambda}_z/c = 0.057$ ,  $\bar{\omega}_p/\bar{\omega}_{e_0} = 0.71$  and  $1.00$ ;  $7^\circ < \theta_0 < 8^\circ$

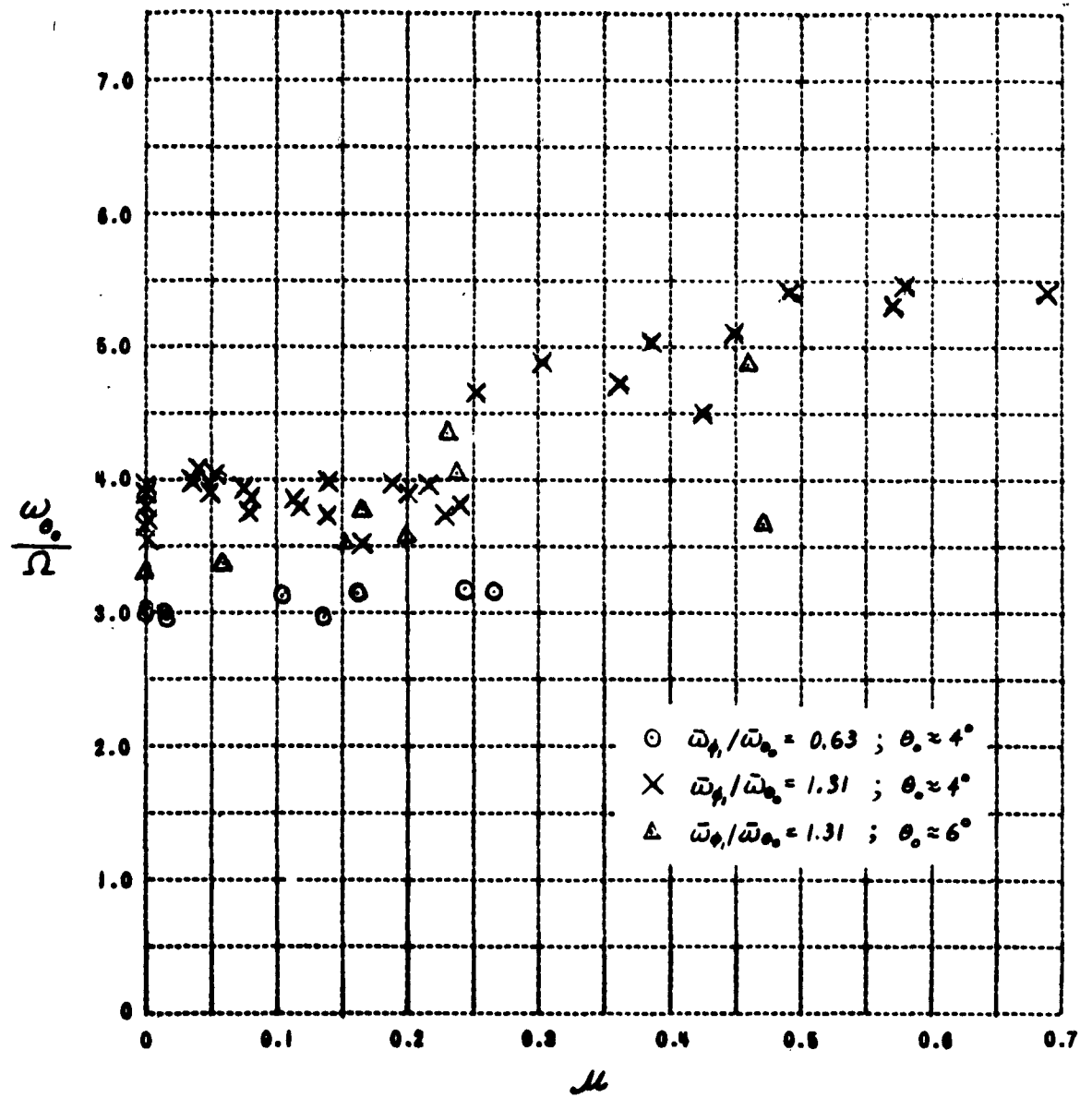


Figure 8e  $\bar{x}_s/c = 0.139$ ,  $\bar{\omega}_1/\bar{\omega}_{0_0} = 0.63$  and  $1.31$ ;  $\theta_0 \approx 4^\circ$

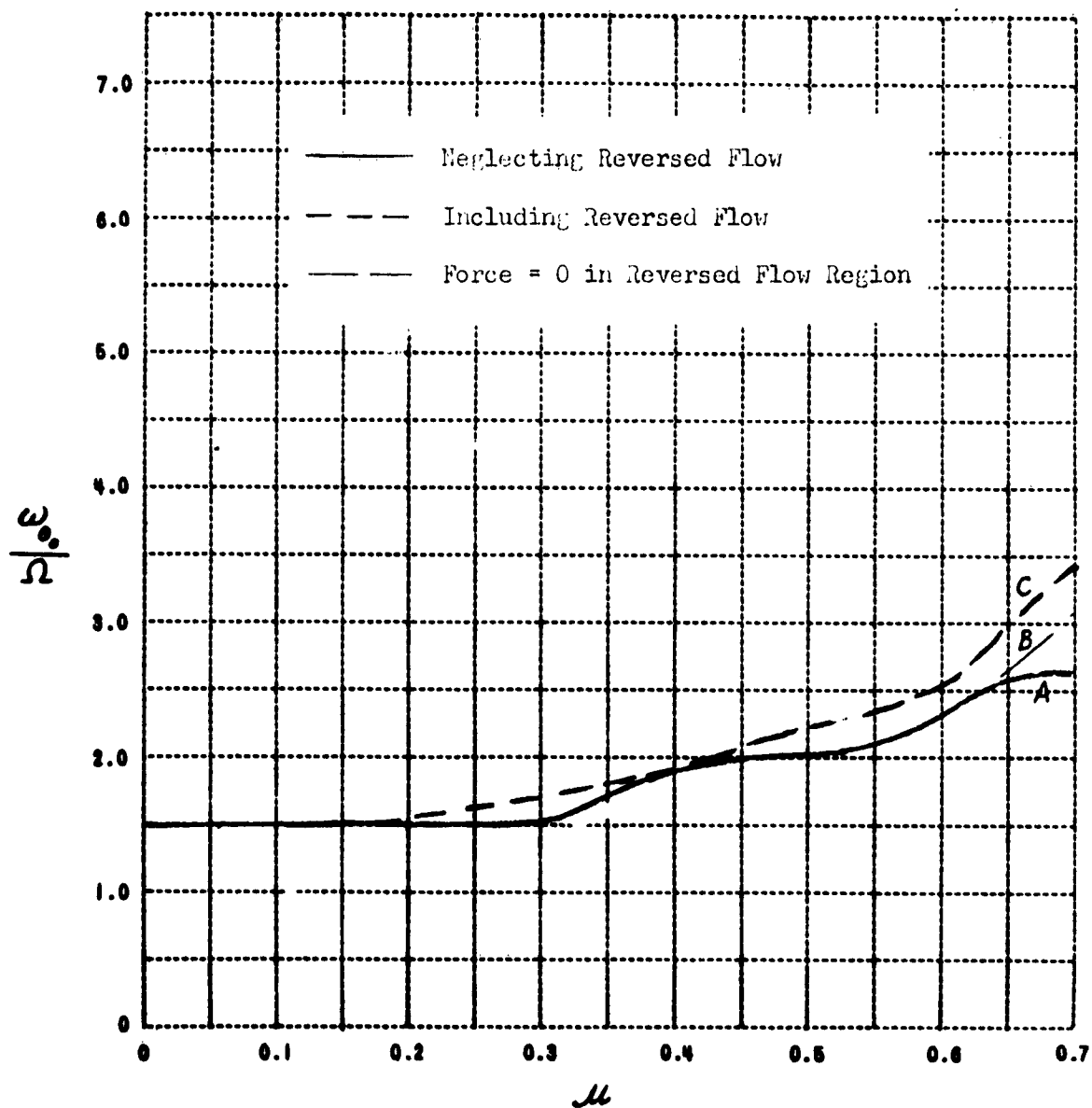


Figure 9a CALCULATED FLUTTER BOUNDARIES: NONROTATING PITCHING  
FREQUENCY/ SHAFT ROTATIONAL SPEED vs ADVANCE RATIO

$$\bar{x}_e/c = 0.0036, \bar{\omega}_H/\bar{\omega}_0 = 1.45$$

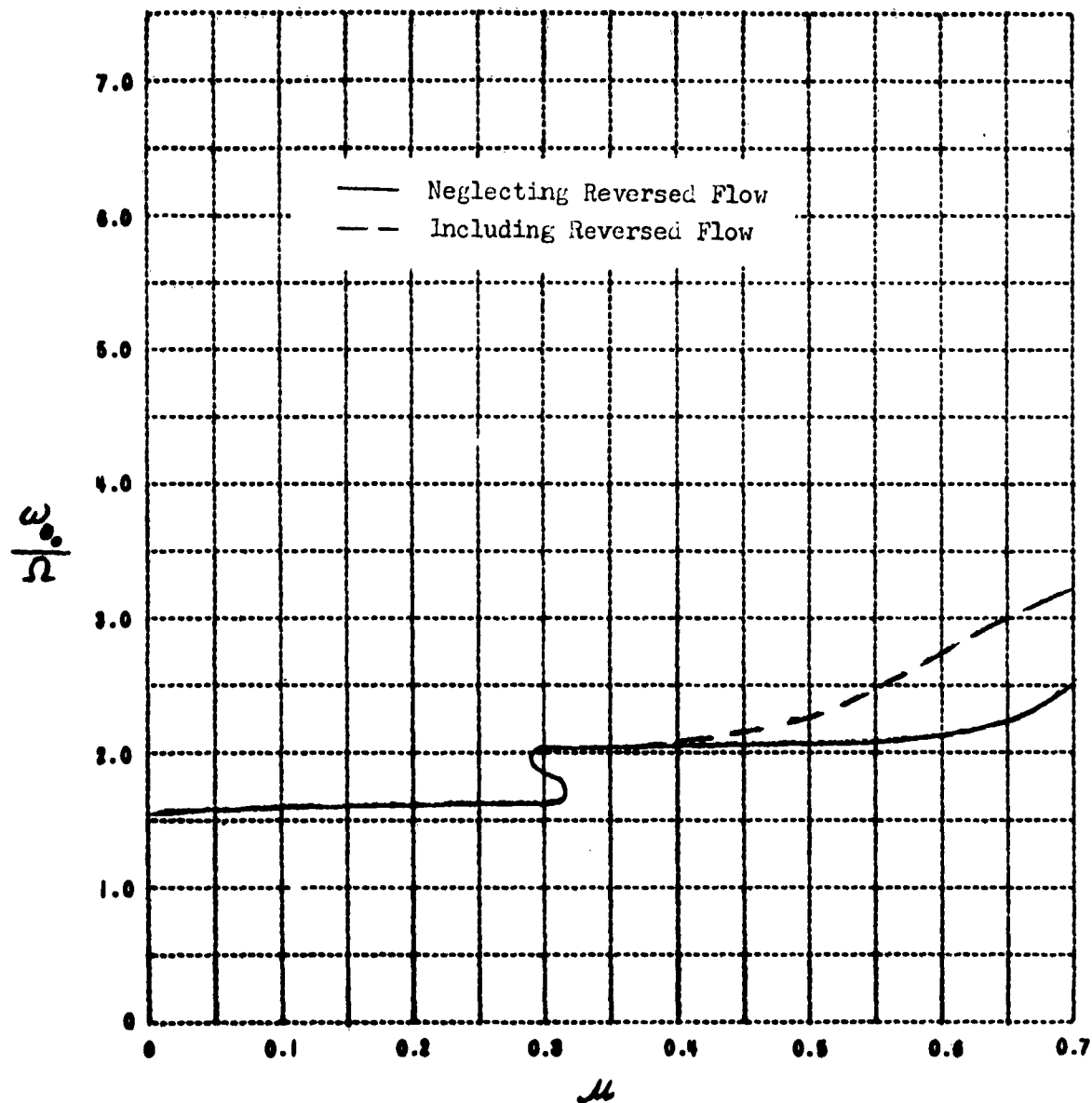


Figure 9b  $\bar{x}_R / C = 0.0036$ ,  $\bar{\omega}_R / \bar{\omega}_{R_0} = 1.04$

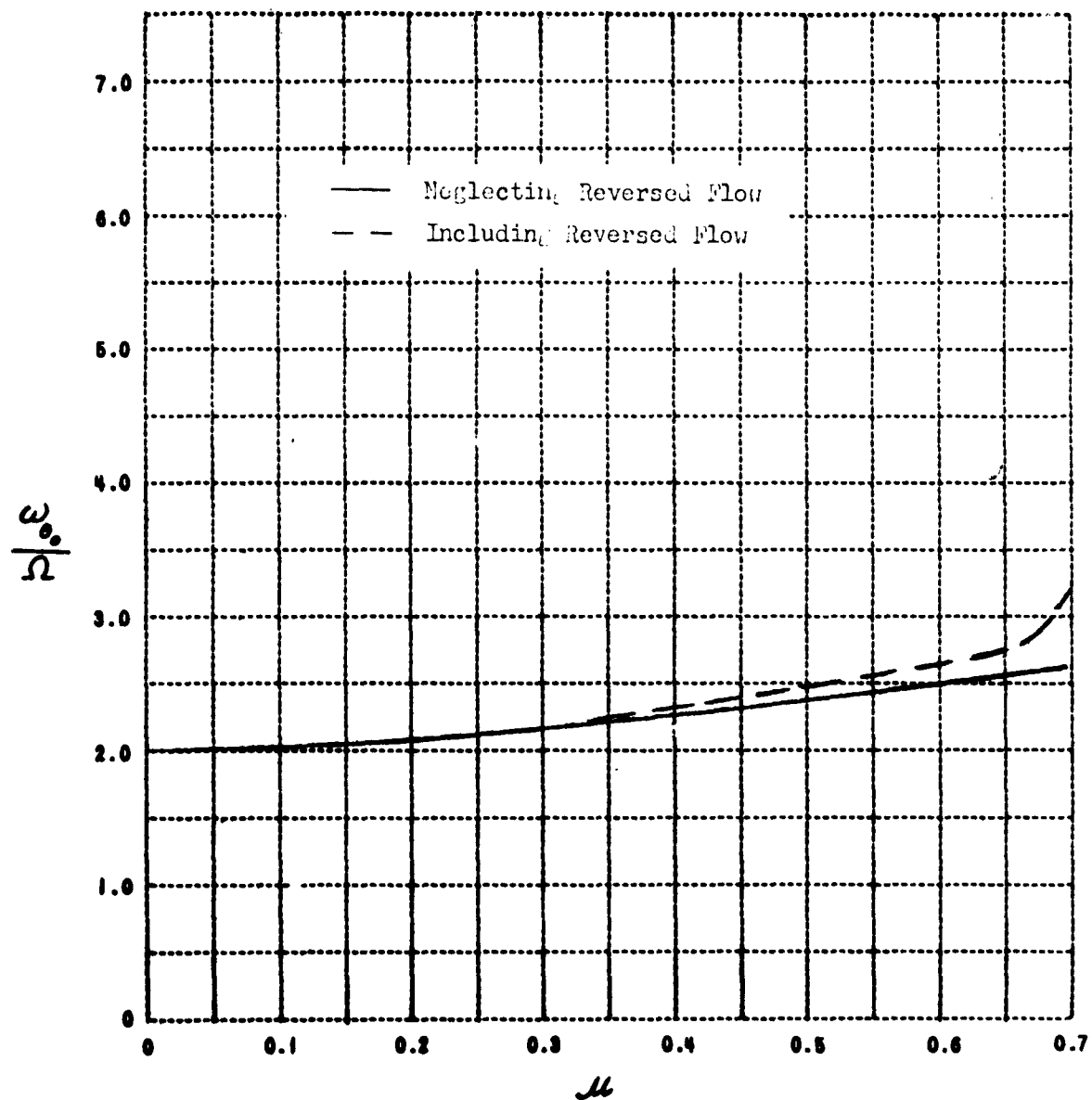


Figure 9c  $\bar{x}_z / c = 0.0036$ ,  $\bar{\omega}_1 / \bar{\omega}_0 = 0.585$

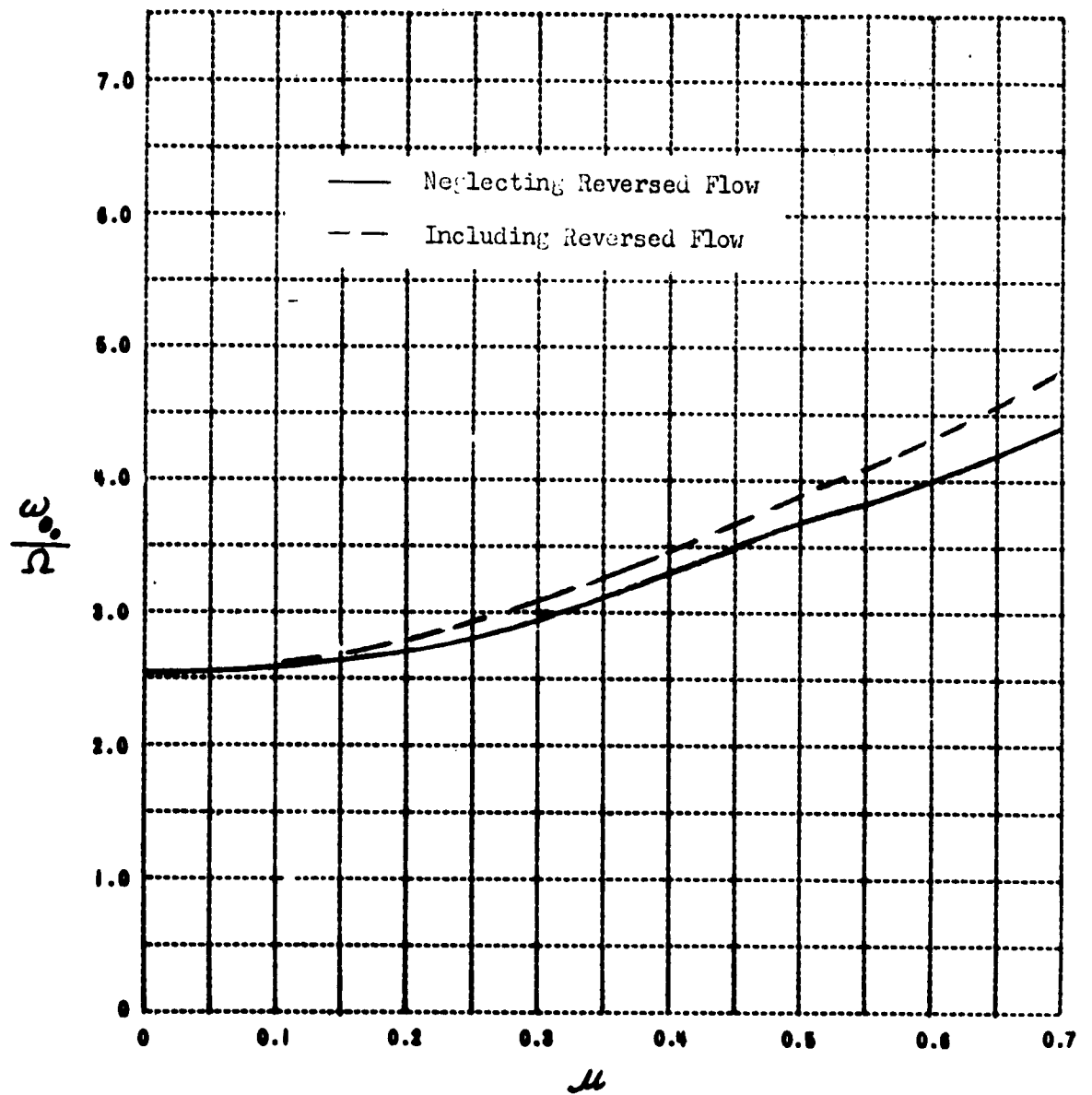


Figure 9d  $\bar{x}_s / c = 0.044$ ,  $\bar{\omega}_s / \bar{\omega}_o = 1.44$

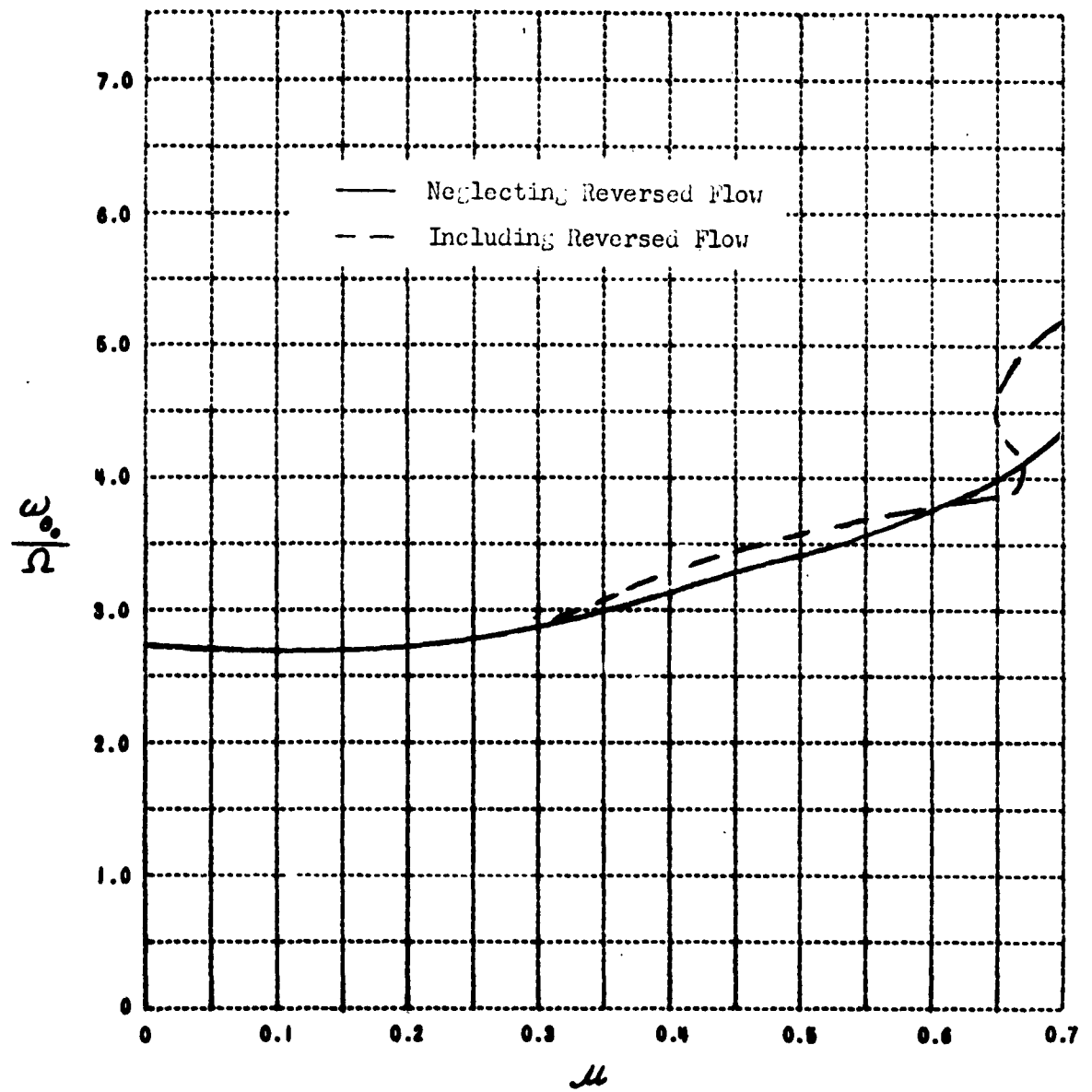


Figure 9e  $\bar{x}_2/c = 0.044$ ,  $\bar{\omega}_1/\bar{\omega}_0 = 0.95$

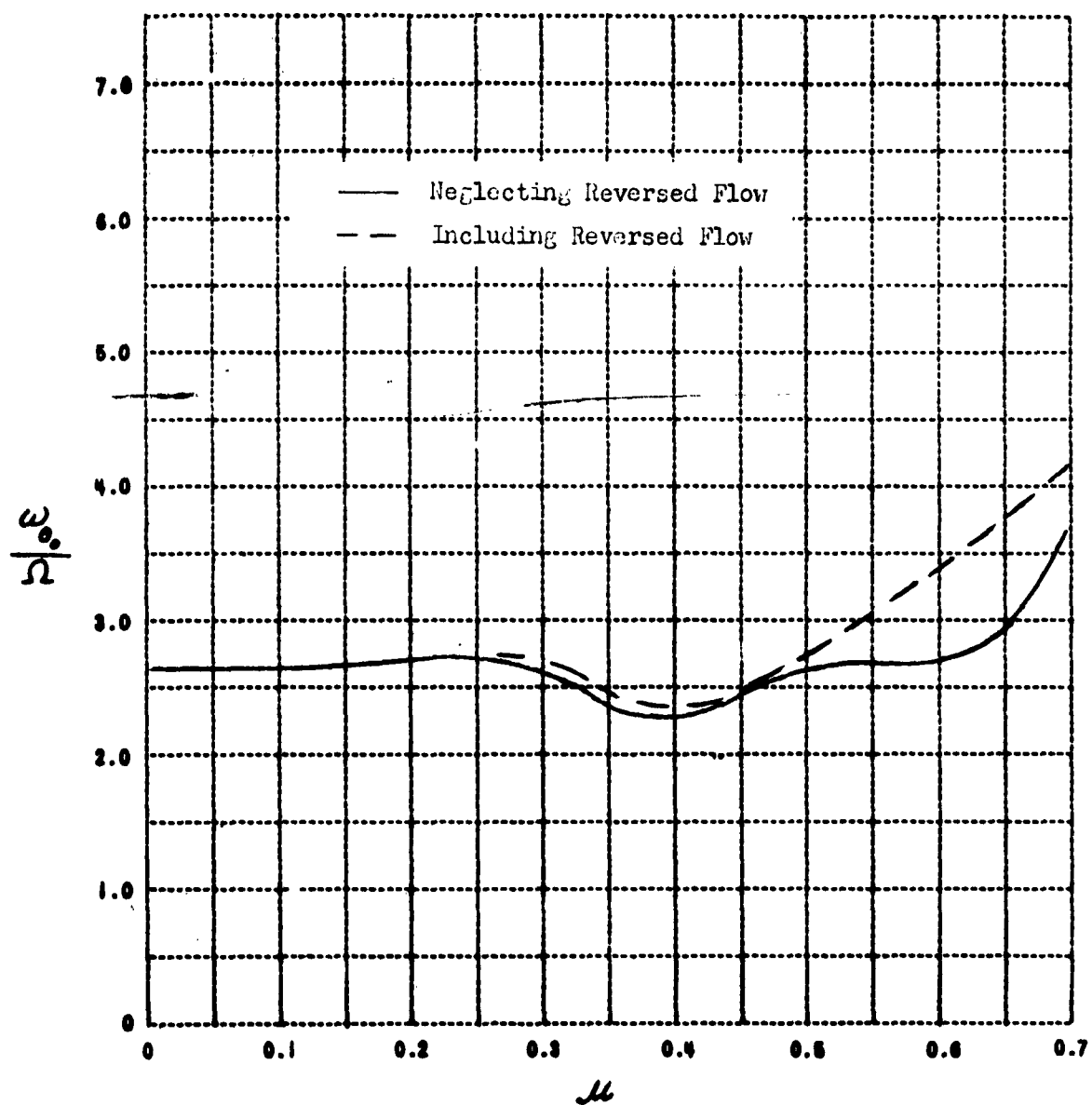


Figure 9f  $\bar{x}_e/C = 0.044$ ,  $\bar{\omega}_b/\bar{\omega}_o = 0.58$

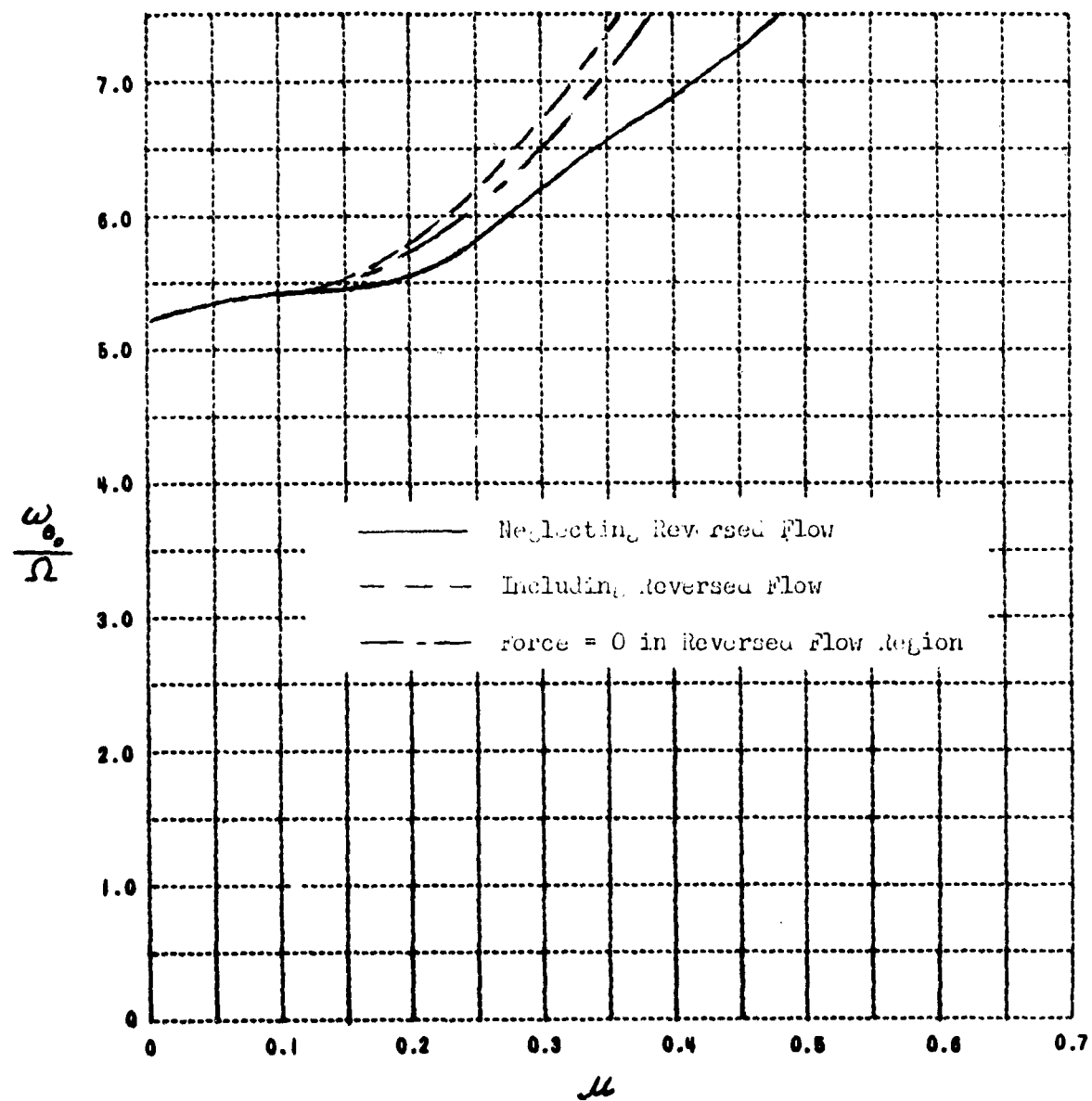


Figure 9g  $\bar{x}_e / c = 0.139$ ,  $\bar{\omega}_h / \bar{\omega}_0 = 1.55$

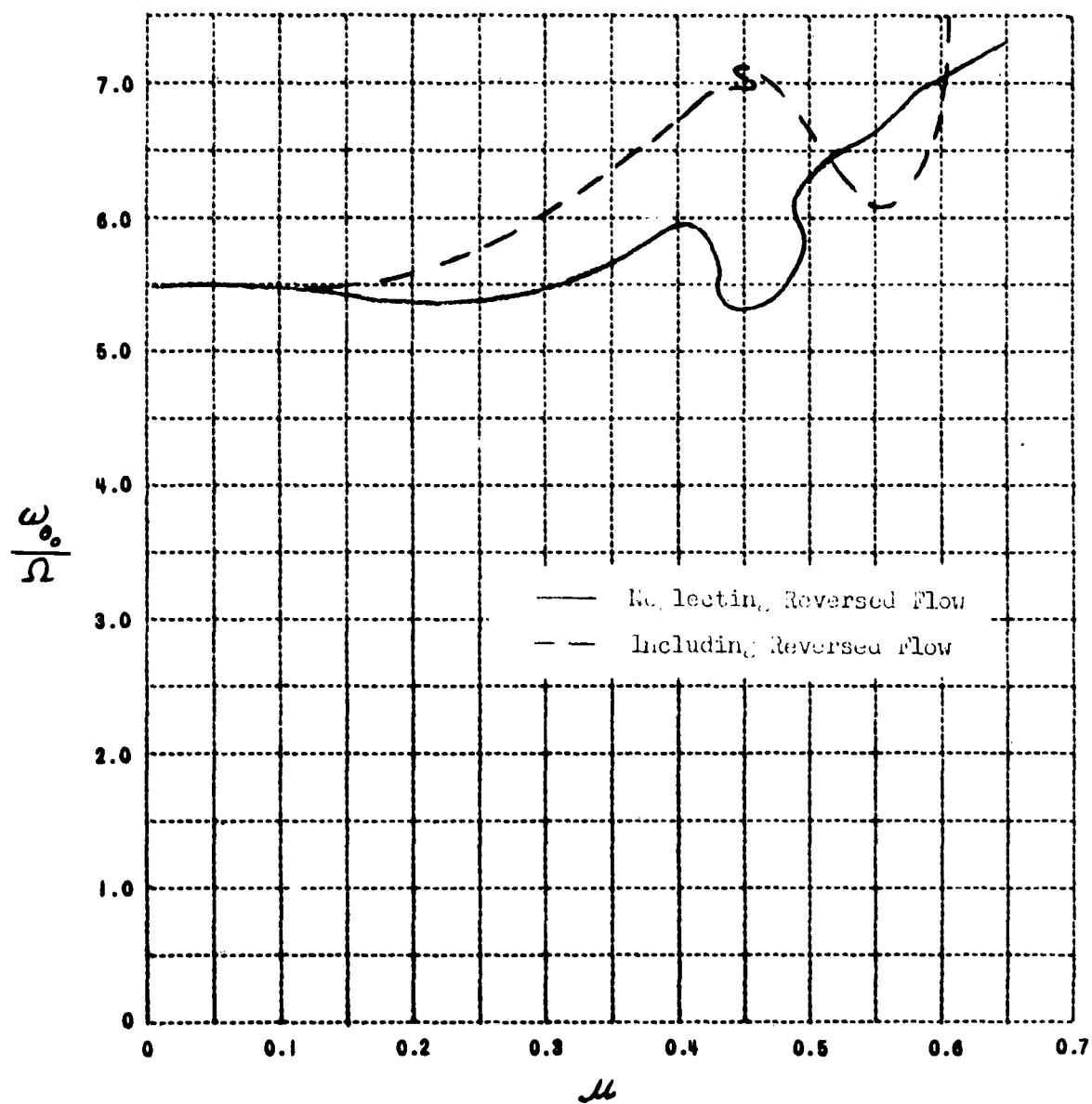


Figure 9h  $\bar{\lambda}_e / C = 0.139$ ,  $\bar{\omega}_h / \bar{\omega}_0 = 1.11$

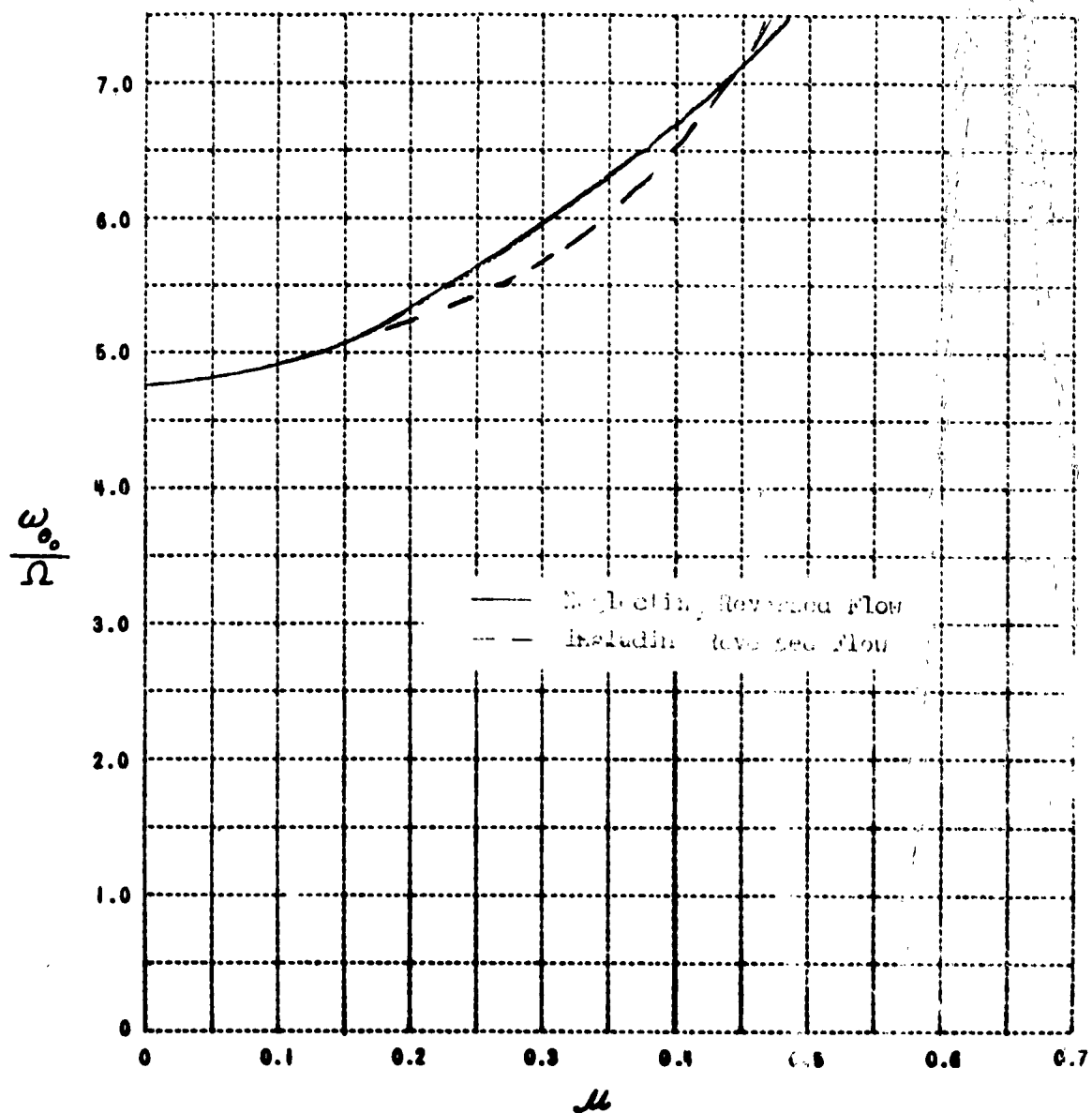


Figure 91  $\bar{x}_e/C = 0.139$ ,  $\bar{\omega}_p/\bar{\omega}_e = 0.3$

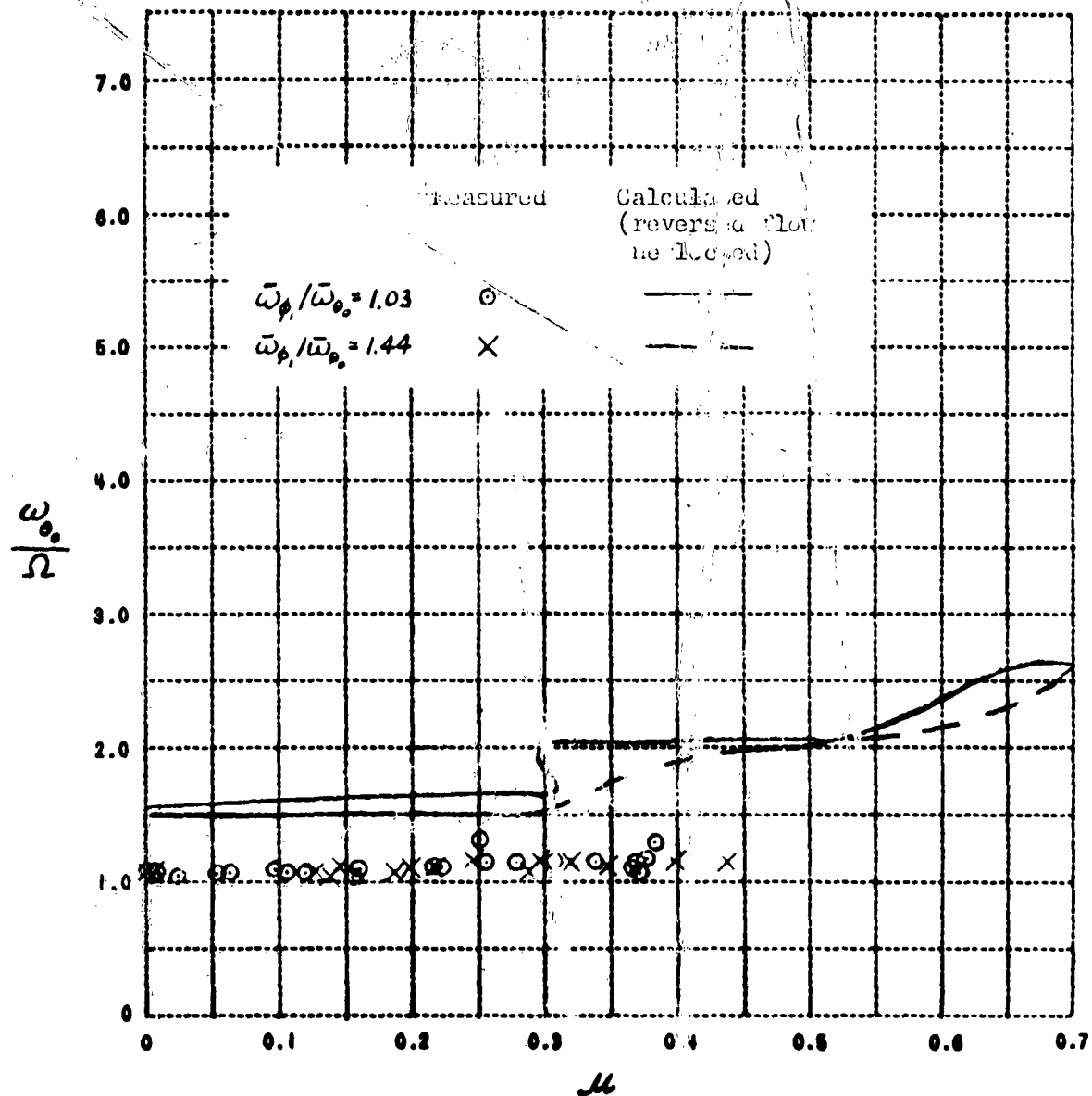


Figure 10a COMPARISON OF EXPERIMENTAL AND CALCULATED FLUTTER BOUNDARIES:  
 [NONROTATING PITCHING FREQUENCY/SHAFT ROTATIONAL SPEED] vs  
 ADVANCE RATIO  
 $\bar{x}_2/c = 0.0036$

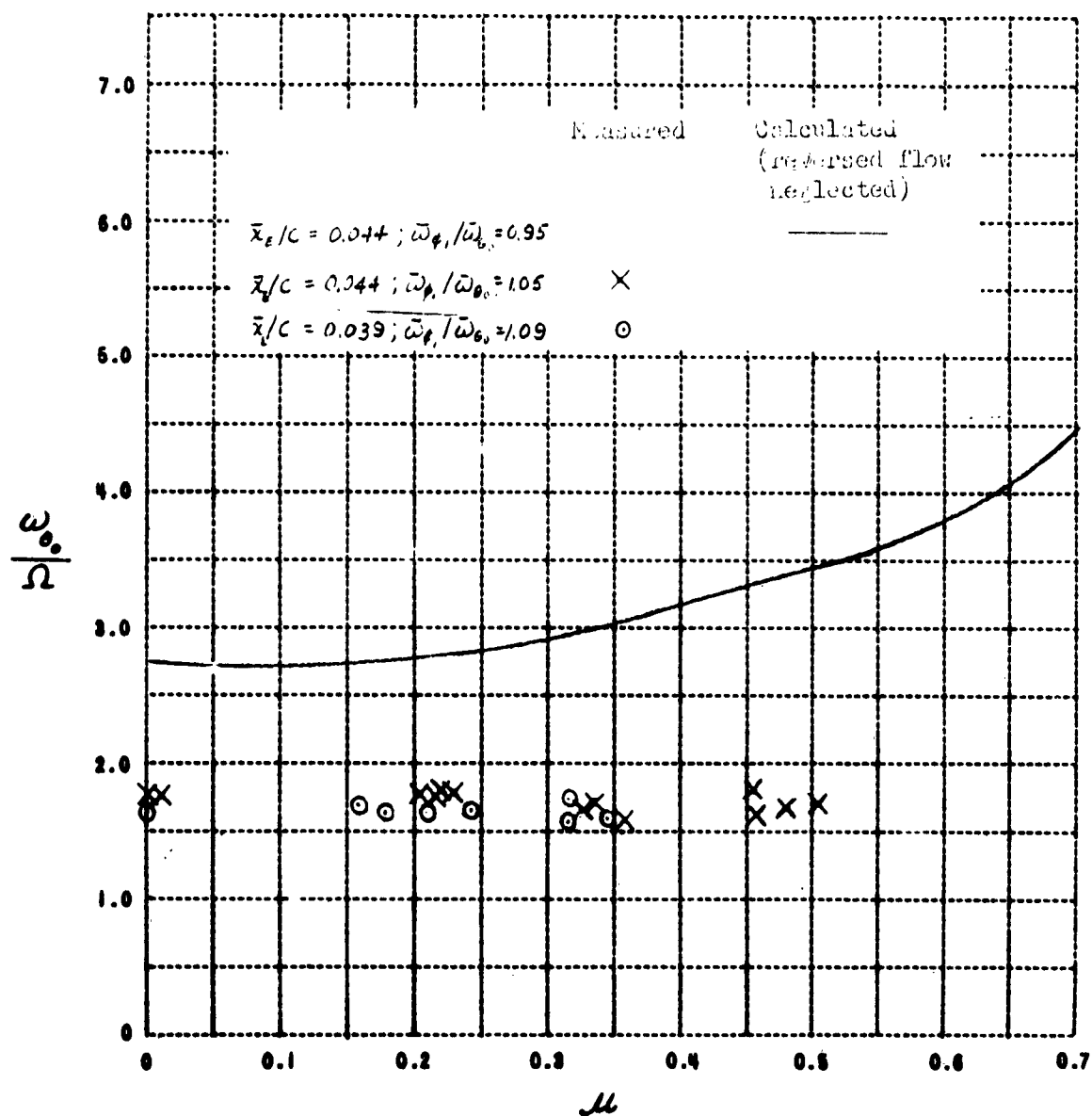


Figure 10b  $\bar{z}_p/c = 0.044$  and  $0.039$

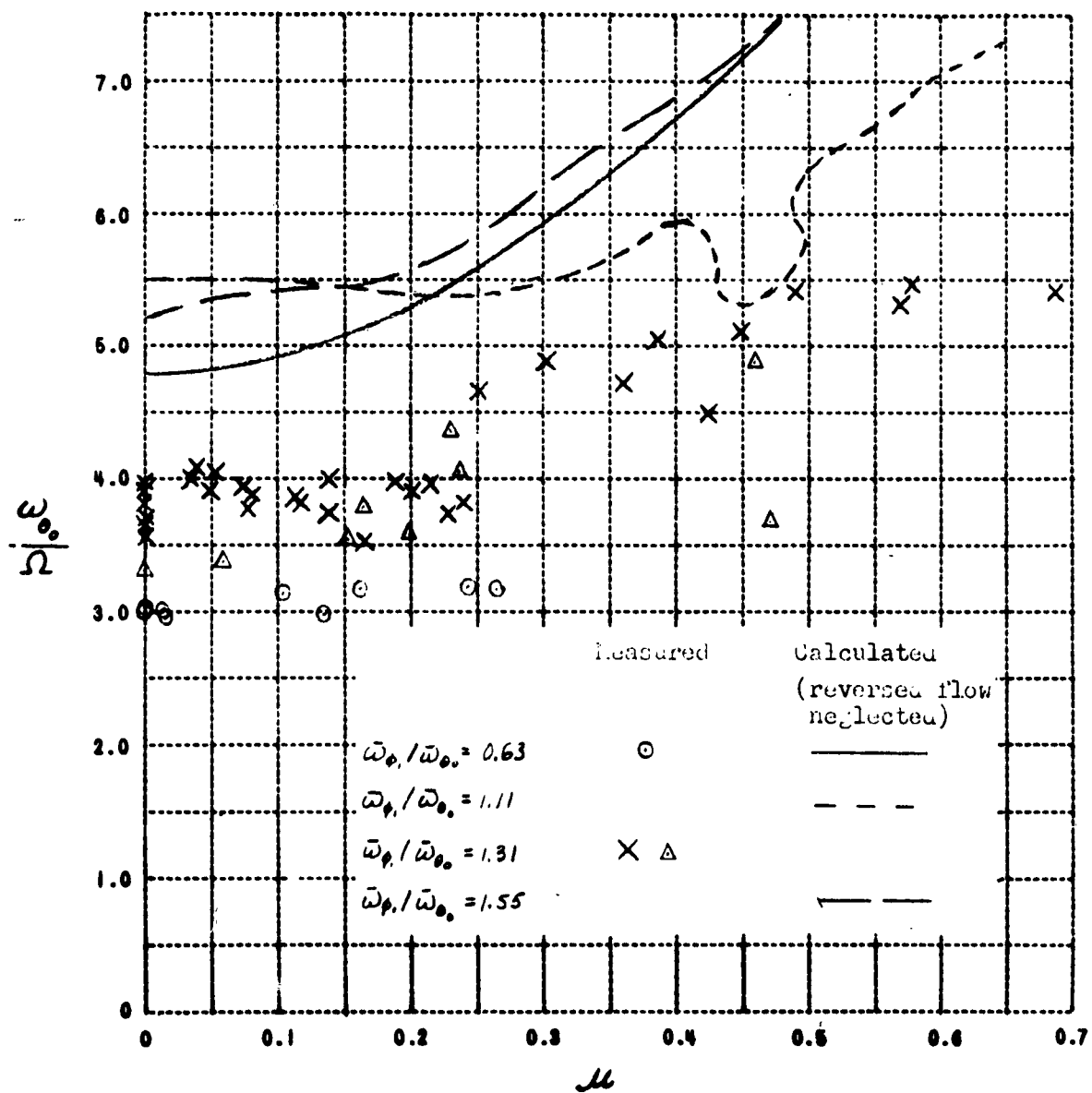


Figure 10c  $\bar{\lambda}_E/c = 0.139$

# REFERENCES

1. DuWaldt, F. A., Gates, C. A., Piziali, R. A. Investigation of the Flutter of a Model Helicopter Rotor Blade in Forward Flight  
WADD TR 60-479 July 1960
2. Frissel, H. Flutter Analysis of Unbalanced Tail Rotor Proposed for R-5 Helicopter  
CAL Report BB-119-M-1 August 1946
3. Daughaday, H. Flutter Analysis of the H-5 Rotor with a Pitch-Cone Coupling Linkage  
CAL Report BB-538-S-3 July 1952
4. DuWaldt, F. A. and Gates, C. An Experimental and Theoretical Study of the Low Frequency Flapping-Pitching Flutter of a Hovering Rotor Blade  
CAL Report SB-680-S-2 September 1952
5. Chang, T. T. A Flutter Theory for a Flexible Helicopter Rotor Blade in Vertical Flight  
CAL Report SB-862-S-1 July 1954
6. Daughaday, H. and Kline, J. An Investigation of the Effect of Virtual Delta-Three Angle and Blade Flexibility on Rotor Blade Flutter  
CAL Report SB-862-S-2 August 1954
7. Daughaday, H., DuWaldt, F. and Gates, C. Investigation of Helicopter Rotor Flutter and Load Amplification Problems  
CAL Report No. SB-862-S-4 August 1956
8. Loewy, R. G. A Two-Dimensional Approximation to the Unsteady Aerodynamics of Rotary Wings  
CAL Report No. 75 October 1955;  
also I.A.S. Preprint No. 605 & Journal of the Aeronautical Sciences  
Vol. 24, No. 2 February 1957
9. Daughaday, H., DuWaldt, F. and Gates, C. Investigation of Helicopter Blade Flutter and Load Amplification Problems  
January 1957; also I.A.S. Preprint No. 705 & Journal of the American Helicopter Society  
Vol. 2, No. 3 July 1957
10. DuWaldt, F. A., Gates, C. A. and Piziali, R. A. Investigation of Helicopter Rotor Blade Flutter and Flapwise Bending Response in Hovering  
WADC Technical Report No. 59-403 August 1959
11. Brooks, G. W. and Sylvester, M. A. The Effect of Control Stiffness and Forward Speed on the Flutter of a 1/10-Scale Dynamic Model of a Two-Bladed Jet-Driven Helicopter Rotor  
NACA Technical Note 3376 April 1955.

# REFERENCES (Cont'd.)

12. Hohenemser, K. H. Remarks on the Unloaded Type of Convertiplane  
Proceedings of the Eleventh Annual Forum, American Helicopter Society  
April 1955
13. Hohenemser, K. H. On a Type of Low-Advance-Ratio Blade Flapping  
Instability of Three-or-More-Bladed Rotors Without Drag Hinges  
Proceedings of the Thirteenth Annual Forum, American Helicopter Society  
May 1957
14. Hohenemser, K. H. and Perisho, C. H. Analysis of the Vertical  
Flight Dynamic Characteristics of the Lifting Rotor with Floating Hub  
and Off-Set Coning Hinges Journal of the American Helicopter  
Society Vol. 3, No. 4 October 1958
15. Chou, P. C. Pitch-Lag Instability of Helicopter Rotors Journal  
of the American Helicopter Society Vol. 3, No. 3 July 1958
16. McKee, J. W. Pitch-Lag Instability as Encountered During Tests  
of a Model Rotor Institute of the Aeronautical Sciences Preprint  
No. 807 June 1958
17. Perisho, C. H. Analysis of the Stability of a Flexible Rotor  
Blade at High Advance Ratio Journal of the American Helicopter  
Society Vol. 4, No. 2 April 1959
18. Shulman, Y. Stability of a Flexible Helicopter Rotor Blade in  
Forward Flight Journal of the Aeronautical Sciences July 1956
19. Sullivan, E. M. A Test Apparatus for Small Rotorcraft Vol. I  
Development and Operational Checkout CAL Report No. SG-1195-S-3  
November 1959
20. Laitone, E. V. and Talbot, Lawrence Subsonic Compressibility  
Corrections for Propellers and Helicopter Rotors Journal of the  
Aeronautical Sciences Vol. 20, No. 10 October 1953